CHALMERS
UNIVERSITY OF TECHNOLOGY

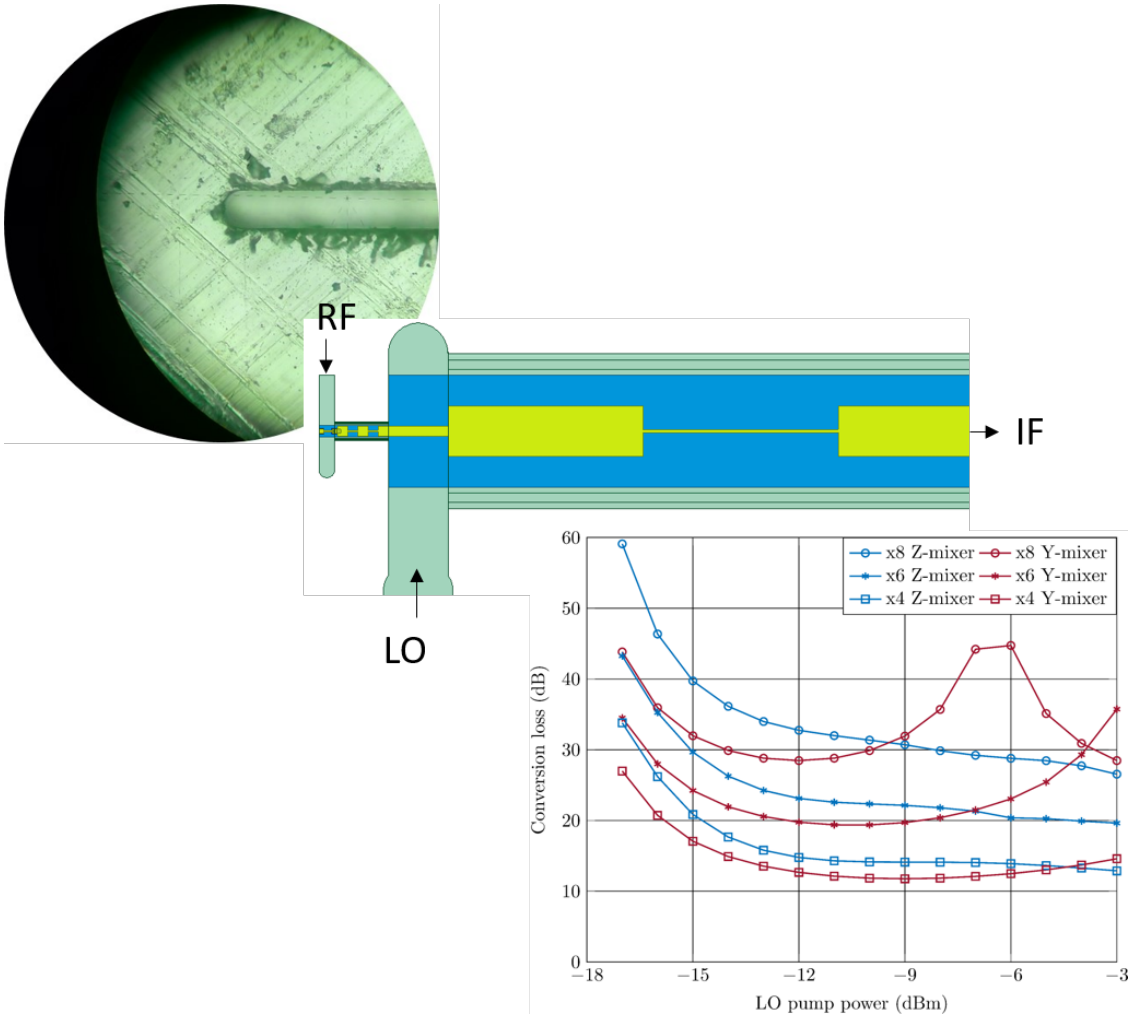

Design and modeling of terahertz Schottky diode harmonic mixers

Master's thesis in Wireless, Photonics and Space Engineering

DIVYA JAYASANKAR

Department of Microtechnology and Nanoscience - MC2
CHALMERS UNIVERSITY OF TECHNOLOGY
Gothenburg, Sweden 2019

Master's thesis 2019

Design and modeling of terahertz Schottky diode harmonic mixers

DIVYA JAYASANKAR

CHALMERS
UNIVERSITY OF TECHNOLOGY

Department of Microtechnology and Nanoscience
Terahertz and Millimetre Wave Laboratory
Chalmers University of Technology
Gothenburg, Sweden 2019

Design and modeling of terahertz Schottky diode harmonic mixers
Divya Jayasankar

Supervisor: Peter Sobis, Omnisys Instruments AB
Examiner: Jan Stake, Terahertz and Millimetre Wave Laboratory

Master's Thesis 2019
Department of Microtechnology and Nanoscience
Terahertz and Millimetre Wave laboratory
Chalmers University of Technology
SE-412 96 Gothenburg
Telephone +46 31 772 1000

Cover: a) Picture showing the E-plane split block of RF waveguide operating at 3.5 THz, b) 3D-electromagnetic model of x6 harmonic mixer design showing the input RF, LO signal and output intermediate frequency signal, c) Plot showing conversion loss of x4, x6 and x8 Schottky-diode based harmonic mixers versus LO operating power.

Typeset in LaTeX
Printed by Chalmers Reproservice
Gothenburg, Sweden 2019

Design and modeling of terahertz Schottky diode harmonic mixers
DIVYA JAYASANKAR
Department of Microtechnology and Nanoscience - MC2
Chalmers University of Technology

Abstract

Compact, efficient and reliable frequency converters, preferably operating at room temperature are necessary for frequency stabilising far infra-red optical sources inorder to achieve high spectral resolution. Future air and space-borne instrumentation requirements are driven by the need to accommodate compact LO sources for detection of atomic oxygen (OI) and hydroxyl radical (OH) lines at 3.5 THz, and 4.7 THz as they provide valuable information in atmospheric and planetary sciences. The main objective of this work is to design and model Schottky diode-based harmonic mixers for phase locking of quantum cascade laser operating at 3.5 THz. Detailed large-signal analysis of the four basic single-ended Z-, H-, G-, and Y-mixers was carried out using a standard Schottky-diode model to determine the optimum diode embedding impedances and mixer performances. Conversion nulls were observed in Y-mixers due to destructive interference among the mixing products. It is noticed that for low local oscillator pump power, Y-mixer has low conversion loss. However, as the local oscillator pump power increases, Z-mixer provides reduced conversion loss due to the associated power dissipation in the idler circuits. Based on the ideal simulation study, a 3D electromagnetic model of planar single-ended Schottky diode with sub-micron anode size, integrated with suspended strip-lines on an ultra-thin GaAs membrane was designed. The estimated conversion loss for x6 harmonic mixer operating at 3.5 THz is around 35 dB for −4 dBm local oscillator pump power including the waveguide losses.
The designed x6 harmonic mixer is intended to be a part of the quantum cascade laser frequency stabilization scheme operating at 3.5 THz in the proposed European Space Agency's mission LOCUS (Linking Observations of Climate, the Upper atmosphere, and Space weather) targeting the mesosphere and lower thermosphere region (MLT). This thesis also provides initial guidelines for a x8 harmonic mixer design operating at 4.7 THz.

Keywords: Conversion efficiency, far-infrared, frequency converters, frequency stabilization, harmonic mixers, phase-locking, Schottky diodes, diode mixers.

Acknowledgements

Foremost, I would like to express my sincere gratitude to Prof. Jan Stake for giving me this opportunity to work on this project. It was great working with you and thanks for all the fruitful discussions we had, your motivation and guidance helped me to finish this project successfully.
I would like to thank Adj. Prof. Peter Sobis who provided insight and expertise that greatly assisted this project work. I would also like to thank Dr. Tomas Bryllert and Dr. Josip Vukusic for insightful comments and encouragement throughout the project. My sincere thanks also go to Vladimir Drakinskiy for diode fabrication and Mats Myremark for precision waveguide-milling. I would like to thank Dr. Elena Saenz, European Space Agency and Dr. Heinz-Wilhelm Hübers, German Aerospace Centre for all fruitful discussions.
This research was carried out in the Gigahertz Centre in a project financed by European Space Agency under the contract No. 4000125911/18/NL/AF, "Frequency stabilisation of a Quantum Cascade Laser for Supra-THz applications" and Swedish National Space Agency under the contract No. 170/17, "THz Schottky diode mixers for high-resolution FIR spectroscopy".

Divya Jayasankar, Gothenburg, June 2019

Contents

List of Figures

List of Tables

List of Abbreviations

CAD	Computer Aided Design
DSB	Double Side-Band
EM	Electro-Magnetic
ESA	European Space Agency
FEM	Finite Element Method
FET	Field Effect Transistor
GaAs	Gallium Arsenide
HB	Harmonic Balance
HEB	Hot Electron Bolometer
IC	Integrated Circuit
IF	Intermediate Frequency
L_m	Mixer Conversion Loss
LNA	Low Noise Amplifier
LO	Local Oscillator
LOCUS	Linking Observations of Climate, the Upper atmosphere and Space weather
MMIC	Microwave Monolithic Integrated Circuit
PLL	Phase Locked Loop
QCL	Quantum Cascade Laser
RF	Radio Frequency
VNA	Vector Network Analyzer
VSWR	Voltage Standing Wave Ratio
SiO_2	Silicon dioxide
SIS	Superconductor-Insulator-Superconductor
SSB	Single Side-Band
S-parameter	Scattering parameter

List of Notations

k_B	Boltzmann's constant
η	Diode ideality factor
w_d	Depletion width
q	Elementary charge
σ	Electrical conductivity
μ_n	Electron mobility
V_F	Forward-bias voltage
μ_p	Hole mobility
C_j	Junction capacitance
μ_0	Magnetic permeability of free space
ϵ	Permittivity
h	Planck's constant
V_R	Reverse-bias voltage
R_s	Series resistance
c	Speed of light in vacuum
δ_s	Skin depth
C_{j0}	Zero-bias junction capacitance

Constants

c	$2.9979 \times 10^{8}\,\mathrm{m/s}$
h	$6.6260 \times 10^{-34}\,\mathrm{m^2\ kg/s}$
k_B	$1.3806 \times 10^{-23}\,\mathrm{m^2\ kg\ s^{-2}\ K^{-1}}$
μ_0	$4\pi \times 10^{-7}\,\mathrm{H\ m^{-1}}$
ϵ_0	$8.8541 \times 10^{-12}\,\mathrm{F\ m^{-1}}$
q	$1.6021 \times 10^{-19}\,\mathrm{coulombs}$

1

Introduction

The terahertz frequency range in the electromagnetic spectrum is located between 300 GHz to 10 THz. Due to technical advancement in the past decade, terahertz technology is finding use in a very wide range of applications: plasma diagnostics, medical imaging, remote sensing, climate monitoring [1]-[2]. Measurements of molecular spectral lines at sub-millimetre wavelength provides valuable information about stellar evolution, cosmic chemistry, planetary and atmospheric sciences [3]. Despite it's interesting scientific potential, terahertz spectrum is least explored due to unavailability of sources, components at high frequencies. However, due to the recent development in device fabrication techniques [4]-[5], precision waveguide milling, advancements in commercial electromagnetic simulation softwares and availability of terahertz sources: frequency multipliers [6], quantum cascade lasers [7] has paved way for the development of high spectral resolution heterodyne spectrometers [8]-[9]. Scientists have become increasingly interested in detection of molecular lines at terahertz frequencies. Future air/space-borne instruments requires compact solutions for atmospheric measurements of atomic oxygen (OI) and hydroxyl radical (OH) at 3.5 THz and 4.7 THz respectively [10]. Much research has examined ultra-low noise terahertz technology like superconductor-insulator-superconductor (SIS) [11] and hot electron bolometer mixers (HEB) [12] as they offer high receiver sensitivity. However, there is a strong need for compact terahertz heterodyne receivers with high spectral resolution that are able to operate without any cryogenic cooling.

Schottky diode technology is robust and can operate over a wide temperature range, intermediate frequencies and is hence attractive for space instrumentation. Since passive cooling is sufficient, Schottky diode technology is better suited for long lifetime missions compared to cryogenic technology. Schottky barrier is formed due to the metal-semiconductor junction, Braun [13] was the first to study rectification property in metal-semiconductors in 1874. Later in 1904, a physicist from India named Bose developed semiconductor diode detectors operating at 60 GHz [14]. In the year 1937, Walter H. Schottky, a German physicist proposed that the current rectification in the metal-semiconductor junctions is caused by the potential barrier that exists in the semiconductor-metal interface. This potential barrier was later named as Schottky-barrier. Planar Schottky diodes with integrated circuit technology has led to the development of reliable and advanced terahertz mixers and multipliers with better performance [15] compared to the whisker-contacted devices [16]. In 1999, Siegel et al.[17] demonstrated membrane based technology that allows for low electrical parasitics and operation at terahertz frequencies. Based on this monolithic membrane diode technology, the first planar 2.5 THz Schottky diode heterodyne receiver was developed for a NASA spaceflight mission using a CO_2 pumped

methanol far-infrared laser [18]. However, the lack of efficient and compact power sources [19] above 2 THz, is one of the limiting factors that restrict the realization of un-cooled heterodyne receivers at higher frequencies [20].
Over the past decade, Quantum Cascade Lasers (QCLs) has shown steady improvement in performance [7], thereby making it an ideal candidate as a compact local oscillator source for room temperature Schottky diode receivers. However, due to the frequency drift in terahertz laser sources caused by temperature and driving current variation, it is critical to frequency stabilize the quantum cascade lasers [21]. Frequency stabilization can be achieved by locking the QCL frequency to the molecular transition [22], using a precise frequency comb [23]. However, for long-time space mission, the most reliable method is to lock the QCL frequency to a stable microwave reference signal. Phase locking of QCL using a super-lattice mixer was demonstrated by [24] at 4.7 THz with a SNR of 20 dB for 30 kHz resolution bandwidth. Phase locking using a Schottky diode-based harmonic mixers was demonstrated by [25], with the Schottky diode technology developed at the Chalmers University of Technology. Conversion loss of 27 dB and 30 dB was measured for 3^{rd} and 4^{th} harmonic mixing respectively. Fabrication process involves electron-beam lithography with a beam spot less than 5 nm thereby allowing precise anode contact and air-bridge formation.
The main objective of this project is to design a Schottky diode based x6 harmonic mixer which has low conversion loss and high signal to noise ratio in-order to achieve phase locking of QCL at terahertz frequencies. Moving up in frequency, circuit losses increases therefore it is crucial to accurately model the effects of parasitics, and reduce the substrate loss. Also, progressing high in frequency, the performance of the diode mixer is significantly limited by noise temperature, power-coupling bandwidth and high frequency losses. The design is based on Schottky diodes with sub-micron anode area, defined using nano lithography techniques, and integrated with suspended striplines on an ultra-thin GaAs-membrane.
In this work, frequency stabilization of QCL will be achieved by locking the frequency to a stable microwave reference source. By utilizing the higher harmonic (x6) of the LO signal (585 GHz), RF signal can be down-converted to a low intermediate frequency. A digital phase detector will then compare the IF signal to the stable microwave reference signal and produce a dc voltage as feedback thereby stabilizing the frequency of the QCL. Figure 1.1 shows the proposed front-end of the receiver operating at 3.5 THz and 4.7 THz for the LOCUS mission. LOCUS (Linking Observations of Climate, the Upper atmosphere and Space weather) is a proposal for future European Space Agency (ESA) satellite mission to target the mesosphere and lower thermosphere region [26]-[27]. LOCUS mission will have receiver front-ends operating at four terahertz bands: 0.8 THz, 1.1 THz, 3.5 THz, 4.7 THz.

1.1 Thesis outline

Chapter 1 briefly presents the different methods for achieving frequency stabilizing of the terahertz laser sources.
Chapter 2 provides a general description of Schottky diodes and presents results from the theoretical study for estimating the series resistance, junction capacitance and

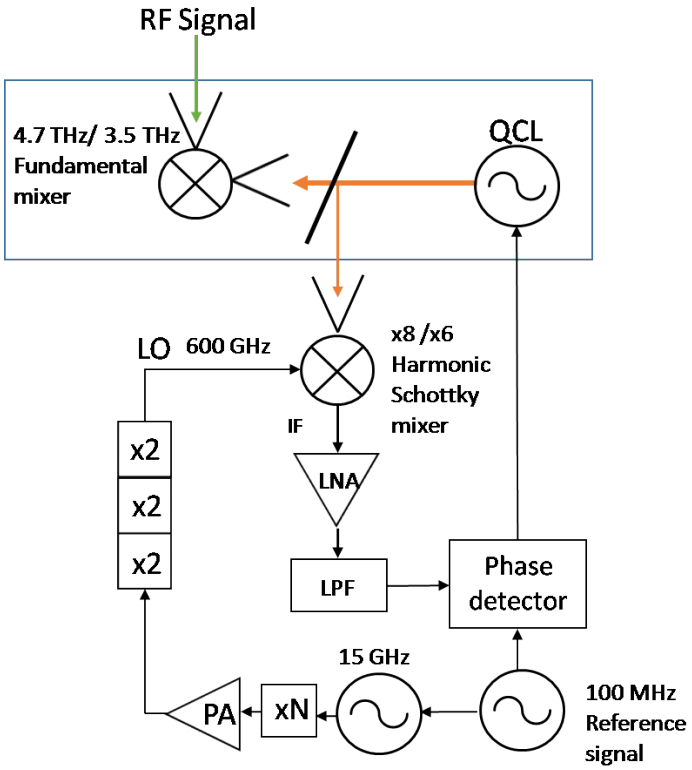

Figure 1.1: Schematic of the front-end receiver operating at 3.5 THz/4.7 THz.

cut-off frequency for different anode contact area and epi-layer doping concentration. Chapter 2, also provides the relevant diode specifications which will be used in the large-signal diode modelling. Finally, a brief introduction to the theory of resistive mixers are provided.
Chapter 3 explains the harmonic balance simulation setup in the circuit simulation setup and gives an overview of the design approach to estimate the optimum diode embedding impedance at RF, LO and intermediate frequencies. Conversion loss for single ended: Z-, H-, G-, Y-mixer circuits from ideal simulation is presented. The later part is about the 3D-electromagnetic modeling of the mixer circuit and conversion loss versus local oscillator power and radio frequency is presented.
Chapter 4 discusses the results obtained from different mixer circuit in the circuit simulation and the results from the EM-modeling. Chapter 5 concludes the thesis work and the planned future work is presented.

2

Theory

The current rectification in metal-semiconductor contact was first observed by Braun in 1874 [13]. The majority carriers in Schottky-diode enables operation at high frequency. Later, Walter H. Schottky postulated that the current rectification in Schottky diode is caused due to the electrostatic potential which arises from the space-region in the semiconductor which is compensated by equal and opposite charge in the metal surface [28]. Figure 2.1a shows the metal and n-type GaAs semiconductor junction. The commonly used Schottky-diode symbol is illustrated in figure 2.1b. Typical metal used for Schottky anode contact is titanium (Ti), platinum (Pt), gold (Au) and chromium (Cr) and for terahertz applications, n-type GaAs is preferred due to its high mobility. For ideal contact, the barrier height is equal to $\Phi_b = \phi_m - \chi_s$ where ϕ_m is the metal-work function and χ_s is the electron affinity in the semiconductor [29]. Usually, the metal-GaAs barrier height is close to 0.8 V.

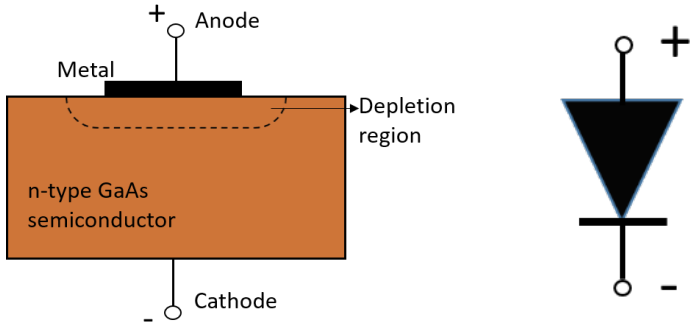

(a) **(b)**

Figure 2.1: a) Metal-semiconductor interface b) Schottky diode symbol

Under thermal equilibrium condition, electrons will flow from the semiconductor to the metal, thereby creating a depletion layer in the semiconductor. Further electron transport from semiconductor is prevented because of the energy barrier created which is also known as built-in potential (ψ_{bi}) as shown in figure 2.2a. Depending upon the voltage applied across the diode terminals, i.e, forward bias and reverse bias, the depletion width (W_d) and the built-in potential (ψ_{bi}) can be altered. When the diode is forward biased, the built-in potential will be lowered by the voltage that is applied across the junction ($\psi_{bi} - V_F$) and the depletion width is narrowed as shown in figure 2.2b. In this condition, the diode operates like a voltage-controlled

resistor mode also called as Varistor (variable resistor). When reverse bias is applied, the energy barrier is increased ($\psi_{bi} - V_R$) and the depletion width gets widened as shown in figure 2.2c, thereby operating as a voltage-controlled capacitor also known as Varactor (variable reactance) [30].

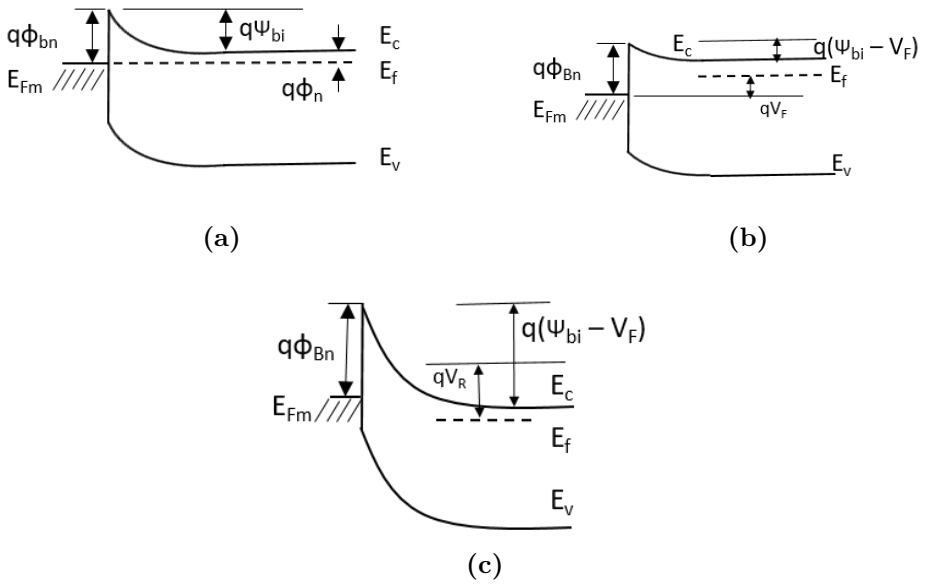

Figure 2.2: Energy band-diagram of n-type GaAs and metal contact for different biasing conditions a) Thermal equilibrium, b) forward bias, c) reverse bias where ψ_{bi} is the built-in potential, V_f is the applied forward bias voltage and V_r is the reverse bias voltage, E_c is the conduction band, E_v is the valence band and E_f is the fermi-level energy band.

Figure 2.3 shows the cross-sectional view of GaAs Schottky diode, anode-pad is formed by metals and epi-layer has n-type GaAs with doping concentration in the range of $3 \times 10^{17}\,\mathrm{cm}^{-3}$ to $5 \times 10^{17}\,\mathrm{cm}^{-3}$, buffer layer facilitates current flow between the epi-layer and the ohmic contact and it is usually doped high (n++ GaAs) with concentration of about $5 \times 10^{18}\,\mathrm{cm}^{-3}$. Ohmic contact allows current flow from the semiconductor to the external circuit.

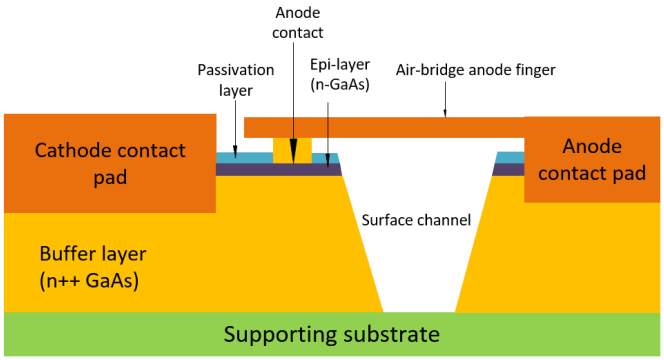

Figure 2.3: Cross-sectional view of GaAs Schottky diode

2.1 Diode equivalent circuit

The lumped equivalent circuit model for a Schottky diode is as shown below in figure 2.4. It consists of a series resistance(R_s), a non-linear junction capacitance (C_j) and non-linear junction conductance (G_j).

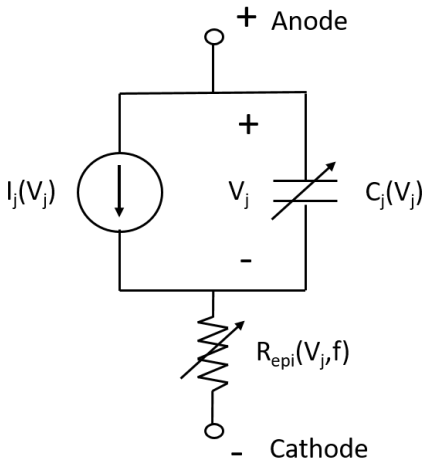

Figure 2.4: Lumped equivalent circuit of GaAs Schottky diode

2.1.1 I-V characteristics

The current-voltage (I-V) characteristics of metal and n-type GaAs Schottky contact is given by

$$I_j(V_j) = I_s(exp^{(\frac{qV_j}{\eta k_B T})} - 1) \tag{2.1}$$

where,

$$I_s = AA^{**}T^2 exp^{(\frac{q\phi_b}{\eta k_B T})}, \tag{2.2}$$

I_j– diode junction current,
I_s – reverse saturation current,
V_j – junction voltage,
η - ideality factor,
A - Anode contact area,
A^{**} - effective Richardson's constant [31],
T - absolute temperature,
ϕ_b - barrier height,

Numerical constants and material properties of GaAs that were used during the calculations are summarized in table 2.1.

Variable name	Description	Value
ψ_{bi}	Built-in potential	0.85 V
η	Ideality factor	1.2
E_g	Bandgap energy	1.42 eV
ϵ_r	Relative dielectric constant	12.9
m_e^*	Effective mass (electrons)	0.063
v_{sat}	Saturation velocity	7×10^6 cm/s
$N_{d_{buffer}}$	Doping concentration in Buffer-layer	$5 \times 10^{18}\,\mathrm{cm}^{-3}$
ρ_c	Specific contact resistance	$10^{-6}\Omega.cm^{-2}$

Table 2.1: Numerical constants and material properties of GaAs

2.1.2 Junction capacitance

The junction capacitance (C_j) can be modelled using parallel plate capacitor approximation. At millimetre and sub-millimetre wavelength, anode radii is small compared to the depletion width and thickness of the epi-layer and the potential in epi-layer is curved near the periphery of the anode. This effect is known as fringing or edge effect and it is important to include these effects in the junction capacitance model [32] as shown below:

$$C_{j0} = \frac{\epsilon_s A}{W}\left(1 + b\left(\frac{W}{R_0}\right)\right) \tag{2.3}$$

where, R_{anode} is radius of the anode contact and b is the numerical constant 1.5. Hence for smaller anodes, a geometry dependent constant $\frac{3\epsilon_s A}{D_{anode}}$ has to be included in the junction capacitance model.
When voltage applied across the diode is varied, then the depletion width will also vary as a function of the junction voltage. The zero-bias capacitance and depletion width can be calculated using the following equations,

$$C_{j0} = Area\sqrt{\frac{q\epsilon_s N_{d_{epi}}}{2\psi_{bi}}} \tag{2.4}$$

$$W_d = \sqrt{\frac{2\epsilon_s \psi_{bi}}{qN_{d_{epi}}}} \tag{2.5}$$

2.1.3 Series resistance

The diode series resistance is one of the important parasitic element that determines the cut-off frequency. The series resistance of a diode comprises of epi-layer resistance, buffer resistance and contact resistance as shown in figure 2.5.

$$R_s = R_{epilayer} + R_{buffer} + R_{contact} \tag{2.6}$$

Epi-layer resistance is caused due to the un-depleted epi-layer and spreading resistance arises due to the current spreading in the buffer layer and contact resistance is between the semiconductor and ohmic contact.

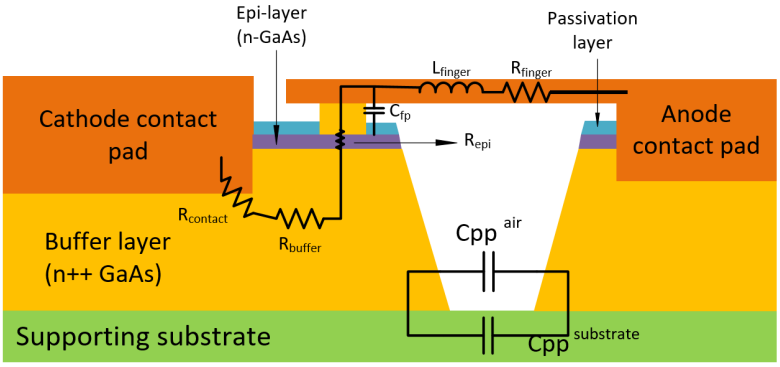

Figure 2.5: Cross-section of GaAs Schottky diode showing the epi, buffer and spreading resistance along with the parasitic capacitances

2.1.3.1 Epi-layer resistance

Epi-layer resistance is calculated using,

$$R_{epilayer} = \frac{t_{epi}}{A\ \sigma_{epi}} \tag{2.7}$$

where, t_{epi} is the thickness of epi-layer and $\sigma_{epi} = q * N_{d,epi} * \mu_{epi}$ is the electrical conductivity of epi-layer, $N_{d,epi}$ and μ_{epi} are doping concentration and mobility of the epi-layer respectively. Electrical conductivity of epi-layer is low compared to the highly-doped buffer region hence the current is assumed to be confined under the anode contact. The thickness of the epi-layer t_{epi} is assumed to be equal to the depletion width when zero-bias voltage is applied [33] refer equation 2.5.

2.1.3.2 Buffer contact resistance

Due to higher electrical conductivity of buffer-layer and larger cathode area, current spreads in the buffer layer and it is usually geometry-dependent. For planar diodes as shown in figure 2.6, the lateral current flow from the anode contact is constricted to the skin-depth in the buffer-layer at 3.5 THz which is about 0.7 µm. This also causes current crowding in the ohmic contact and moving away from the edge, current distribution reduces exponentially and it is called as transfer length L_t [34].

$$R_{buffer} = \frac{1}{\pi\ \sigma_{buffer}\ \delta_s} ln\frac{b}{a} \tag{2.8}$$

where, δ_s is the skin depth at 3.5 THz, a and b are the anode and ohmic contact radius respectively. $\sigma_{buffer} = q\ N_{d,buffer} * \mu_{buffer}$ is the electrical conductivity of buffer layer.

$$\delta_s = \sqrt{\frac{2\ \omega\mu}{\sigma}} \tag{2.9}$$

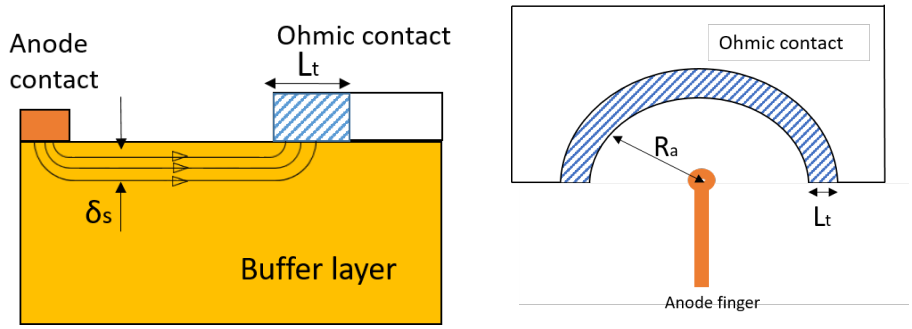

Figure 2.6: Current flow in highly conductive buffer layer for planar diode geometry (side view) and top-view showing the transfer length and effective anode contact area.

2.1.3.3 Ohmic contact resistance

Ohmic contact resistance can be calculated using the formula,

$$R_{contact} = \frac{\rho_c}{A^*_{ohmic}} \tag{2.10}$$

where, ρ_c is the specific contact resistance of n-type GaAs is about 10^{-10} Ωcm^2 and A^*_{ohmic} is the effective ohmic contact area calculated by taking transfer length into account.

2.1.3.4 Low-field mobility model

Doping concentration in epi-layer was varied from $1 \times 10^{16}\,\mathrm{cm}^{-3}$ to $1 \times 10^{18}\,\mathrm{cm}^{-3}$and the anode area was varied between 0.1 um^2 to 0.5 um^2. And,empirical low-field mobility model for GaAs was used to calculate the mobility refer [35] for corresponding doping concentration refer 2.11. Doping concentration and corresponding electron mobility of GaAs at room temperature is shown in figure 2.7.

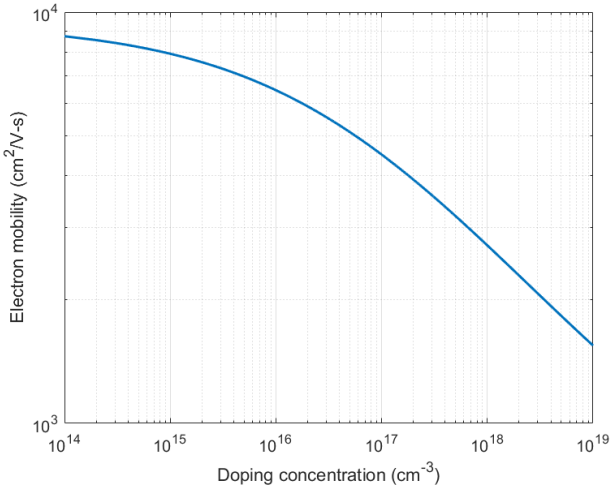

Figure 2.7: Doping concentration vs. electron mobility of GaAs

$$\mu(N,T) = \mu_{min} + \frac{\mu_{max}(300k)(300k/T)^{\theta_1} - \mu_{min}}{1 + \frac{N}{(N_{ref}(300k)(T/300k)^{\theta_2})^{\lambda}}} \tag{2.11}$$

where, θ_1,θ_2 and λ are fitting constants

2.2 Diode cut-off frequency

Cut-off frequency is one of the figure of merit of high-frequency two terminal devices and it can be calculated using the formula as shown below,

$$f_c = \frac{1}{2\ \pi\ R_s\ C_j} \tag{2.12}$$

where R_s is the series resistance and C_j is the junction capacitance [36]. Figure 2.8 shows cut-off frequency contours while anode diameter and epi-layer doping concentration are varied. It is evident that high doping concentration and smaller anode contact is required, in-order to achieve high cut-off frequency.

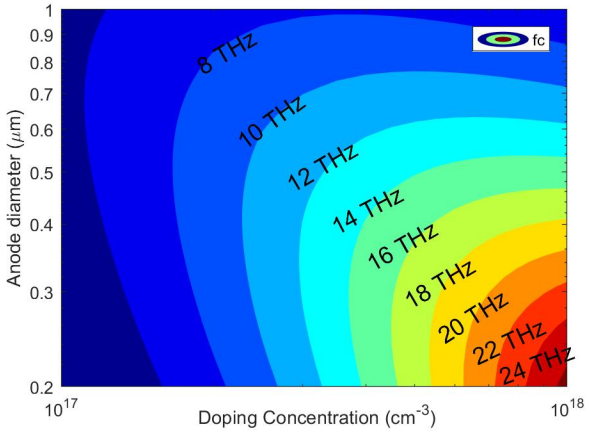

Figure 2.8: Cut-off frequency contours for different epi-layer doping concentration and diameter of anode contact.

2.3 High frequency diode model

Moving higher in frequency, the resistance model is expanded to complex impedance model by including the effects of displacement current, carrier inertia and skin effect [37]. The parallel resonance caused due to the dc-spreading resistance, inertial inductance (L_s) and the displacement capacitance (C_s) as shown in figure corresponds to the plasma resonance [36]. Plasma frequency can be calculated using,

$$\omega_p = \sqrt{\omega_s\ \omega_d} \tag{2.13}$$

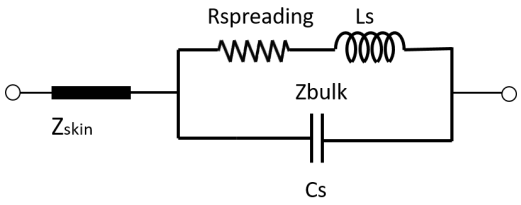

Figure 2.9: High-frequency impedance model in buffer region

where, ω_p, ω_s, ω_d are the plasma frequency, scattering frequency and dielectric relaxation frequency respectively.

$$\omega_s = \frac{q}{m_e^* \mu_n} \tag{2.14}$$

where q is the elementary charge, m_e^* is the effective electron mass and μ_n is the electron mobility in GaAs.

$$\omega_d = \frac{\sigma}{\epsilon_s} \tag{2.15}$$

where, σ is the electrical conductivity and ϵ_s is the dielectric permittivity of GaAs. These frequencies are calculated for different doping concentration and are summarized in the table 2.2. Figure 2.10 shows plasma frequency for varying doping concentrations.

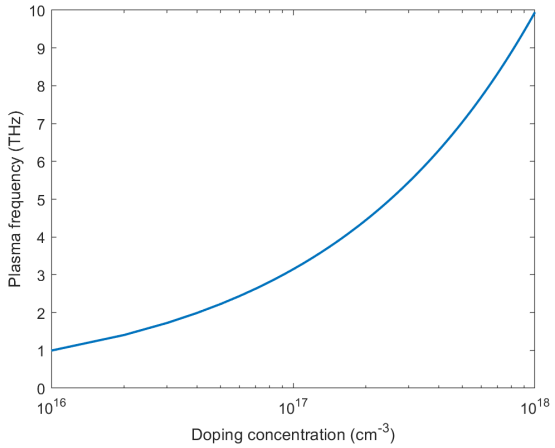

Figure 2.10: Plasma frequency vs. doping concentration

N_d (cm^{-3})	$\frac{\omega_s}{2\pi}$ (THz)	$\frac{\omega_d}{2\pi}$ (THz)	$\frac{\omega_p}{2\pi}$ (THz)
$5\,\mathrm{x}10^{16}$	0.9	5.7	2.2
$3\,\mathrm{x}10^{17}$	1.2	23.8	5.5
$4\,\mathrm{x}10^{17}$	1.3	29.8	6.3
$5\,\mathrm{x}10^{17}$	1.4	35.6	7.0
$6\,\mathrm{x}10^{17}$	1.5	40.9	7.7

Table 2.2: Scattering, dielectric relaxation frequency and plasma frequency for different doping concentration

2.4 Mixer theory

Mixers also called as frequency converters are used to convert high frequency signals to low intermediate frequency signals (down-conversion) using a local oscillator signal which are commonly used in receivers as shown in figure 2.11. In transmitters, they are used to convert a low frequency signal to high radio frequency signal (up-conversion). The frequency conversion is possible due to the non-linear behaviour of the diode [38]. In this work, we use the 6^{th} and 8^{th} harmonic of the local oscillator signal to mix with the radio frequency signal hence they are called as harmonic mixers. It can be seen that from figure 2.11 that if $f_{RF} = f_{LO} - f_{IF} or f_{LO} + f_{IF}$, both the signals will be down-converted to the same intermediate frequency. In a double-sideband (DSB) mixer, both these side-bands are used and are symmetric to the LO signal. In a single-sideband mixer, only one side-band is used and the other side-band is called image frequency. The x6 harmonic mixer described in this thesis, is a single-sideband (SSB) mixer.

$$f_{IF} = f_{LO} - f_{RF} \tag{2.16}$$

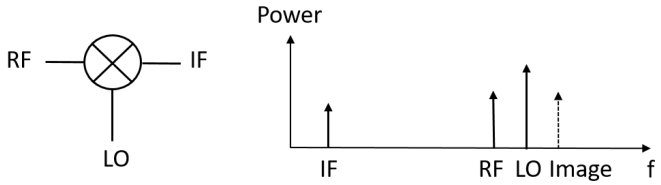

Figure 2.11: Ideal mixer symbol and output spectrum

2.4.1 Single-ended diode mixer

A basic circuit of single-ended diode mixer is shown in figure 2.12. A diplexer is used to combine both high frequency RF signal and LO signal, the diode may be biased with a dc voltage hence a dc blocking capacitor is added that prevents dc leaking into RF path. Similarly, RF choke is added that prevents the RF signal from leaking into the dc path. The output voltage from the mixer is passed through a low-pass filter to provide desired intermediate frequency (IF) as shown in figure 2.12.
Detailed mathematical analysis is presented as follows: Let the input RF voltage be a cosine wave of frequency,

$$v_{RF}(t) = v_{RF}\cos\omega_r t, \tag{2.17}$$

and let the LO input voltage be a cosine wave of frequency,

$$v_{RF}(t) = v_{LO}\cos\omega_l t, \tag{2.18}$$

The total diode current can be expressed as shown below, using the small-signal approximation [39],

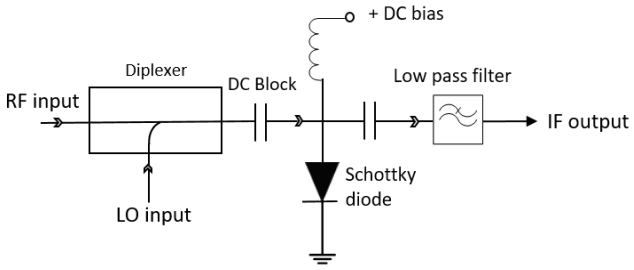

Figure 2.12: Single-ended diode mixer schematic

$$i(t) = I_0 + G_d * (v_{RF}(t) + v_{LO}(t)) + \frac{G'_d}{2}(v_{RF}(t) + v_{LO}(t))^2 \tag{2.19}$$

The first-term, dc bias current will be blocked by the dc block capacitors and the second term will be filtered in a low-pass IF filter and the third term can be re-written as follows.

$$i(t) = \frac{G'_d}{2}[v_{RF}(t) + v_{LO}(t)]^2 \tag{2.20}$$

$$i(t) = \frac{G'_d}{2}[v_{RF}^2 \cos^2\omega_{RF}t + v_{LO}^2 \cos^2\omega_{LO}t]^2 + 2v_{RF}v_{LO}\cos\omega_{RF}t\cos\omega_{LO}t] \tag{2.21}$$

$$\begin{aligned} i(t) = \frac{G'_d}{4}[v_{RF}^2 + v_{LO}^2 + v_{RF}^2\cos(2\omega_{RF}t) + v_{LO}^2\cos(2\omega_{LO}t) \\ +2v_{RF}v_{LO}(\cos(\omega_{LO}t + \omega_{RF}t) + \cos(\omega_{LO}t - \omega_{RF}t))] \end{aligned} \tag{2.22}$$

The dc terms will be blocked by the capacitor and sum frequency ($\omega_{RF} + \omega_{LO}$), $2\omega_{RF}$, and $2\omega_{LO}$ will be filtered by a low-pass filter. Thus, leaving the output intermediate frequency current (ω_{IF}) will be,

$$i_{out}(t) = \frac{G'_d}{2}(2v_{RF}v_{LO}(\cos(\omega_{IF})) \tag{2.23}$$

where, $f_{IF} = f_{LO} - f_{RF}$

2.4.2 Conversion loss

The efficiency of the resistive mixers can be characterized by conversion loss. The single-sideband conversion loss is given by:

$$L_m = P_{RF,in}/P_{IF,out} \tag{2.24}$$

where, $P_{RF,in}$ and $P_{IF,out}$ are input RF frequency and output intermediate frequency [40]. When no energy is dissipated in the out-of-band frequencies (idlers), the theoretical limit on conversion loss is 3 dB. However, it is shown in [41] that when the idlers are reactively terminated, the conversion loss is about 3.92 dB ($20 * log\frac{\pi}{2}$). In reality the conversion loss is degraded due to various factors such as: series resistance, self-heating, parasitic capacitance [42].

2.4.3 Mixer noise

In-order to design the Schottky diode harmonic mixers in an effective way, it is important to analyse the noise performances. Major contributors of noise in Schottky diodes are

- Thermal noise also called as Johnson or Nyquist noise is caused by random fluctuations of electrons [43]-[44].
- Shot noise generated by current flow across the junction

Strutt was the first to investigate about shot noise in mixers [45]. From the lumped equivalent circuit as shown in figure 2.4, each element generates noise. The shot noise current can be modelled as a current source parallel to G_j and thermal noise associated with the series resistance R_s can be modelled as a voltage source series to R_s [40]-[46].

$$\langle i^2 \rangle = 2qi_d\Delta f \tag{2.25}$$

where, i_d is the instantaneous current flow across the junction and the equivalent noise temperature of the junction is given by,

$$T_{shot} = \frac{qV_j}{2k_B} \tag{2.26}$$

The mean square voltage amplitude of thermal noise is given by,

$$\langle v^2 \rangle = 4k_B T_{eff} R_s \Delta f \tag{2.27}$$

where, T_{eff} is the equivalent noise temperature

2.5 Theory of resistive mixers

In a non-linear device, frequency mixing process is achieved by a variable resistance or reactance or combination of both. If the mixing process is achieved by non-linear resistance and some parasitic capacitance, the corresponding mixer is called as the resistive mixer. On the contrary, if the mixing process is accomplished by non-linear reactance and some parasitic reactance, the corresponding mixer is known as parametric mixer. Although, parametric up-converters can produce a power gain, they are unconditionally stable therefore not well-suited for frequency down-conversion applications. Henceforth, resistive mixers are usually preferred for such applications [47]. Schottky barrier diodes are well known for exhibiting purely resistive behaviour [30]. In-order to analyze the resistive mixer performance, the following study was carried out:

1. Classification of the resistive mixers based on the terminations offered to the out-of-band frequencies;
2. Optimum embedding diode impedance at RF, LO and intermediate frequencies that offers least conversion loss;
3. Optimum resistance waveform and pulse duty ratio for corresponding optimum diode embedding network

2.5.1 Classification of mixer circuits

The undesired out-of-band frequencies (idlers) of the resistive mixers can be grouped as one and can be reactively terminated either as a short or as an open circuit also called as unitary division scheme. Saleh [47] has done a detailed analysis on these mixer topologies based on these reactive terminations and classified into two mixers: Z- and Y-mixers in which the out-of-band frequencies are either terminated by a open and a short circuit respectively as shown in figure 2.13-2.14. There are two types of idlers: current and voltage idlers. Current idlers allow current to pass through r(t) in a Z-mixer other than the RF and intermediate frequencies. Voltage idlers allow voltage to exist across g(t) in a Y-mixer for frequencies other than RF and intermediate frequencies. Therefore, Y-mixer with infinite voltage idlers at all out-of-band frequencies can be considered as Z-mixer and vice-versa In the binary division scheme, the frequencies were divided into two groups: even and odd out-of-band frequencies, this resulted in the four basic types of mixers as summarized in table 2.3. The names of these resistive mixers originated from the types of network matrices used to find the mixer performances.

Out-of-band frequencies (ω_{2n})	ω_{2n+1}	Assigned name
Short	Short	Y-mixer
Open	Open	Z-mixer
Open	Short	G-mixer
Short	Open	H-mixer

Table 2.3: Mixer classification based on out-of-band frequency terminations: Binary division scheme

The mixer circuit in which all the out-of-band frequencies are terminated with open circuit is known as Z-mixer as shown in 2.13. The filters on each side of r(t) presents open circuit to all frequencies except the RF and intermediate frequency. For Y-mixer, all the out-of-band frequencies are terminated with a short circuit as illustrated in figure 2.14 and the filters will provide short circuit to all frequencies except the RF and intermediate frequency.

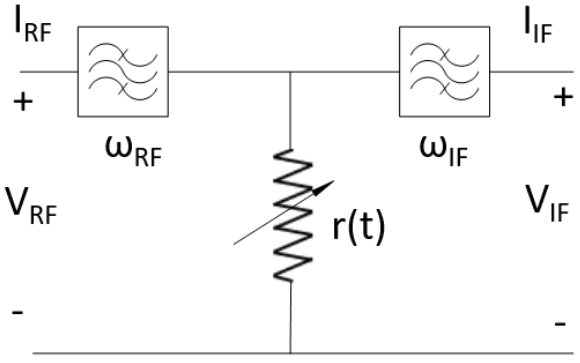

Figure 2.13: Z-mixer - Out of band frequencies are open circuited

The Z-matrix is given by,

$$\begin{bmatrix} V_{RF} \\ V_{IF} \end{bmatrix} = \begin{bmatrix} r_{11} & r_{12} \\ r_{21} & r_{22} \end{bmatrix} \begin{bmatrix} I_{RF} \\ I_{IF} \end{bmatrix} \tag{2.28}$$

In order to evaluate the performance of a Z-mixer, impedance (Z)-matrix is required hence the name[47]. If the image frequency is treated differently from the rest of the out-of-band frequencies, then a three port equation must be applied as shown below:

$$\begin{bmatrix} V_{RF} \\ V_{IF} \\ V_{Image} \end{bmatrix} = \begin{bmatrix} r_{11} & r_{12} & r_{13} \\ r_{21} & r_{22} & r_{23} \\ r_{31} & r_{32} & r_{33} \end{bmatrix} \begin{bmatrix} I_{RF} \\ I_{IF} \\ I_{Image} \end{bmatrix} \tag{2.29}$$

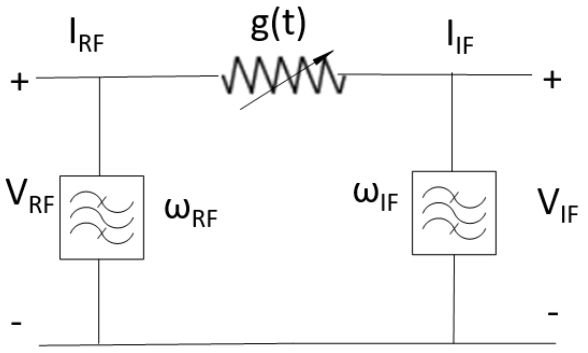

Figure 2.14: Y-mixer - Out of band frequencies are short circuited

Similarly for Y-mixers,

$$\begin{bmatrix} I_{RF} \\ I_{IF} \end{bmatrix} = \begin{bmatrix} g_{11} & g_{12} \\ g_{21} & g_{22} \end{bmatrix} \begin{bmatrix} V_{RF} \\ V_{IF} \end{bmatrix} \tag{2.30}$$

2.5.2 Optimum resistance waveform

For a given optimum embedding diode impedance network and reactive termination of out-of-band frequencies, it is important to analyse the optimum resistance waveform that varies from R_{low} and R_{high} that provides the least mixer conversion loss. For Z-mixer, consider the non-linear resistance varies between $0 \leq r(t) \leq \infty$. where,

$$r(t) = r_o + 2 * r_1 * cos(\omega_p t) + .. \tag{2.31}$$

The optimum conversion loss is given by,

$$L_{opt} = \frac{1 + \sqrt{1 - \epsilon}}{1 - \sqrt{1 - \epsilon}} \tag{2.32}$$

where, $\epsilon = \frac{r_1}{r_o}^2$ and $r_1 > 0$. In order to have minimum conversion loss, ϵ should be maximized. The optimum resistance waveform can be found by solving the equation stated below:

$$\frac{r_1}{r_o} = \frac{\int_{-\pi}^{\pi} r(t)cos(w_{lo}t)dw_p t}{\int_{-\pi}^{\pi} r(t)dw_{lo}t} \tag{2.33}$$

$R_{low} \leq r(t) \leq R_{high}$

$$r(t) = R_{high} \qquad \mid t \mid \leq \frac{\Delta}{2\omega_{LO}} \tag{2.34}$$

$$r(t) = R_{low} \qquad \frac{\Delta}{2\omega_{LO}} \leq \mid t \mid \leq \frac{\pi}{\omega_{LO}} \tag{2.35}$$

And, Δ can be found by solving the transcendental equation shown below,

$$tan(\frac{\Delta}{2}) = \frac{\Delta}{2} + \frac{\pi R_{low}}{R_{high} - R_{low}} \tag{2.36}$$

By solving the above equation, the optimum resistance waveform for Z-mixer and Y-mixer is as shown in figure 2.15-2.16.

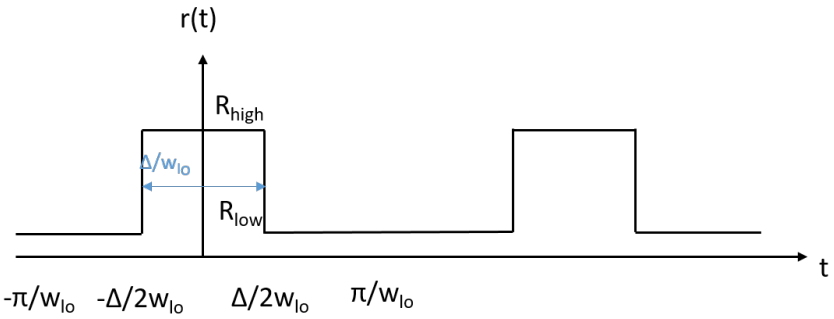

Figure 2.15: Optimum resistance waveform for Z-mixer

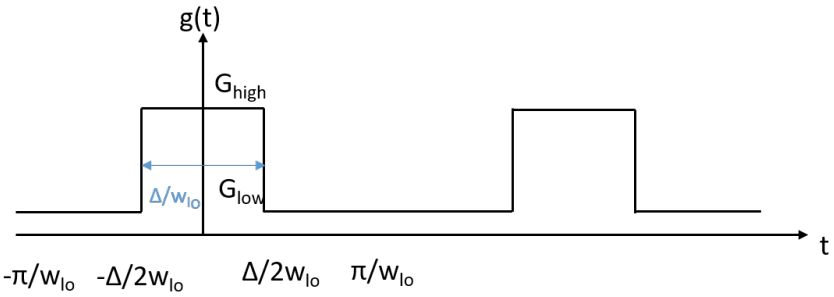

Figure 2.16: Optimum conductance waveform for Y-mixer

The optimum conversion loss equation can be re-written as,

$$L_{opt} = \frac{1 + sin(\Delta/2)}{1 - sin(\Delta/2)} \tag{2.37}$$

2.6 Literature study on Schottky diode mixers

Schottky diode technology is the workhorse behind broadband sub-mm hetrodyne radiometers, operating at ambient temperatures. They operate in wide intermediate frequency range, robust and better suited for long lifetime missions compared to other technologies that requires cryogenic cooling [11]. Whisker contact Schottky diode based mixers were widely used in heterodyne receivers, they offer very low parasitic capacitances. Peatman *et al.* demonstrated a 0.5 µm GaAs Schottky barrier diodes for low-noise terahertz receiver applications with zero biased capacitance of about 0.5 fF [48]. However, whisker contact diodes are not reliable and unable to withstand vibrations and hence not suitable for space missions, In 1987 Bishop *et al.* proposed a new whisker contact-less Schottky diode technology, paving the way for the development of robust, reliable and mechanically stable Schottky-diode structures [49].
Ali-Ahmad *et al.* in 1993 demonstrated a planar, low-noise Schottky receiver with quasi-integrated horn antenna operating at 250 GHz, and exhibited a conversion loss of 7.2 dB and noise temperature of about 1310 Kelvin at 258 GHz operating at room temperature [50]. In 1996 Petri *et al.* designed a planar single-ended Schottky diode-based mixer for ODIN satellite, operating at 119 GHz using micro-strip technology and achieved a conversion loss of about 7 dB and SSB noise temperature 900 Kelvin at room temperature [51]. In 1994, Räisännen *et al.* developed a sub-harmonic anti-parallel Schottky barrier diode operating at 220 GHz, placed in a novel split-waveguide block technology which had conversion loss of 10 dB and single side-band noise temperature of 2000 Kelvin from 210 GHz to 235 GHz.
Though the planar Schottky diode technology has led to a tremendous development in building compact, integrated receiver systems, higher shunt capacitances can severely affect the performance of the diode at terahertz frequencies. A lot of research has been carried out to improve the performance of Schottky-diodes from late 1990's, by accurately modeling the parasitic effects [52], to reduce the substrate loss by using MOMED (Monolithic membrane diode) [17] and substrate-less technology [53].
In 2012, Zhao *et al.* from Chalmers University of Technology has demonstrated a GaAs monolithic membrane-diode mixer operating at 557 GHz, with state of the art performance with 9 dB conversion and DSB noise temperature of 1100 Kelvin [54]. This design employs an anti-parallel sub-harmonic membrane Schottky barrier diode fabricated using electron beam lithography process [5]. In 2018, Arvid *et al.* presented the development of 874 GHz receiver for the (ISMAR) International Submillimetre Airborne Radiometer. It has integrated horn antenna, a dielectric lens, Schottky diode-based mixer circuit, and an integrated low-noise integrated amplifier circuit [55] in a metal split-waveguide block with a DSB noise temperature of about 3300 Kelvin.

3
Method

This chapter describes the Schottky diode technology, diode modeling and harmonic balance simulation setup in the circuit simulator to find the optimum embedding impedances at RF, LO and intermediate frequencies. Based on this, a full 3D-electromagnetic model was designed in finite element method simulator. This chapter also presents the geometry optimization and parametric sweep that were carried out in the design process in-order to achieve desirable mixer performances.

3.1 Design requirements

The Schottky diode-based x6 harmonic mixer is intended to meet the following requirements as summarised in the table below,

Conversion loss	DSB noise temperature	RF, LO, and Intermediate frequencies	Instantaneous bandwidth
40 dB	< 35,000 Kelvin	3.5 THz, 585 GHz, and 10 GHz	1 GHz

Table 3.1: Design requirements for x6 Schottky-based harmonic mixer

3.2 Design methodology

The following design approach was carried out to design the x6 harmonic mixer operating at 3.5 THz. Harmonic balance simulations were performed to study four basic mixer configurations: Z-, H-, G-, and Y-mixer. The diode embedding impedances at LO, RF, and intermediate frequencies were optimized in-order to achieve the least conversion loss. The transmission loss in waveguides, including horn antennas, are very high at terahertz frequencies and it is therefore essential to find a compact circuit solution with short access waveguides. Moreover, the short wavelengths (86 µm) set narrow fabrication tolerances. Therefore, a single ended mixer topology was chosen. The mixer has E-plane split block configuration, since it is easier to mill the waveguide and waveguide channels. Planar diode geometry optimization [56] and tuning of back-short length was carried out, in-order to present the optimum embedding impedance to the diode at RF frequency. Planar stepped impedance filter was chosen, as it is easier to design and fabricate which acts as a band-stop filter preventing the leakage of the RF and LO signal. LO matching was achieved with a quarter-wave waveguide transformer and reduced height LO waveguide section. A horn antenna will be integrated as a part of the waveguide housing [57] as well as

a low noise amplifier MMIC for the IF signal [58] but it is beyond the scope of this thesis. The design approach is divided into three sub-sections as follows:

Diode selection

- Estimate the diode area (A), epi-layer doping concentration N_d, thickness of the epi-layer t_{epi} such that it offers low parasitic capacitances and maximize the cut-off frequency;
- Calculate the diode series resistance R_s and junction capacitance C_j from the analytical model;

Mixer topology

- Find the optimum out-of-band frequency terminations for single-ended diode mixer;
- Optimize the diode embedding impedance at LO, RF and IF frequencies in-order to get minimum conversion loss;

3D electromagnetic modeling

- Design of RF and LO waveguides operating at 3.5 THz and 585 GHz respectively;
- Electromagnetic modeling of planar Schottky diode structure;
- Present the desired RF optimum embedding impedance to the diode by tuning the length of the back-short and geometry optimization of the diode structure;
- Design of stepped impedance planar filter structure to prevent the leakage of RF and LO signal;
- Design of quarter-wave waveguide transformer to present the optimum diode impedance at LO frequency.

3.3 Diode technology

Realization of circuits at high frequencies are often limited due to the existence of higher order propagating modes in the supporting GaAs substrate. In-order to reduce the circuit losses and parasitics, the integrated diode technology will be realized using suspended stripline technology in 2 µm thick GaAs membrane [5]. The Chalmers Schottky diode process has shown state-of-the-art performance in various receivers between 183 GHz and 3 THz [55], [59], [25]. Figure 3.1 shows the scanned electron microscope picture of sub-micron anode size Schottky diode fabricated at Chalmers University of Technology.

3.4 Schottky diode model

From the theoretical study, following important conclusions were made,

- Anode contact area should be preferably less than 0.2 µm^2, Epi-layer doping concentration should be higher than 5×10^{17} cm^{-3} to reduce the parasitics and to operate below the cut-off frequency

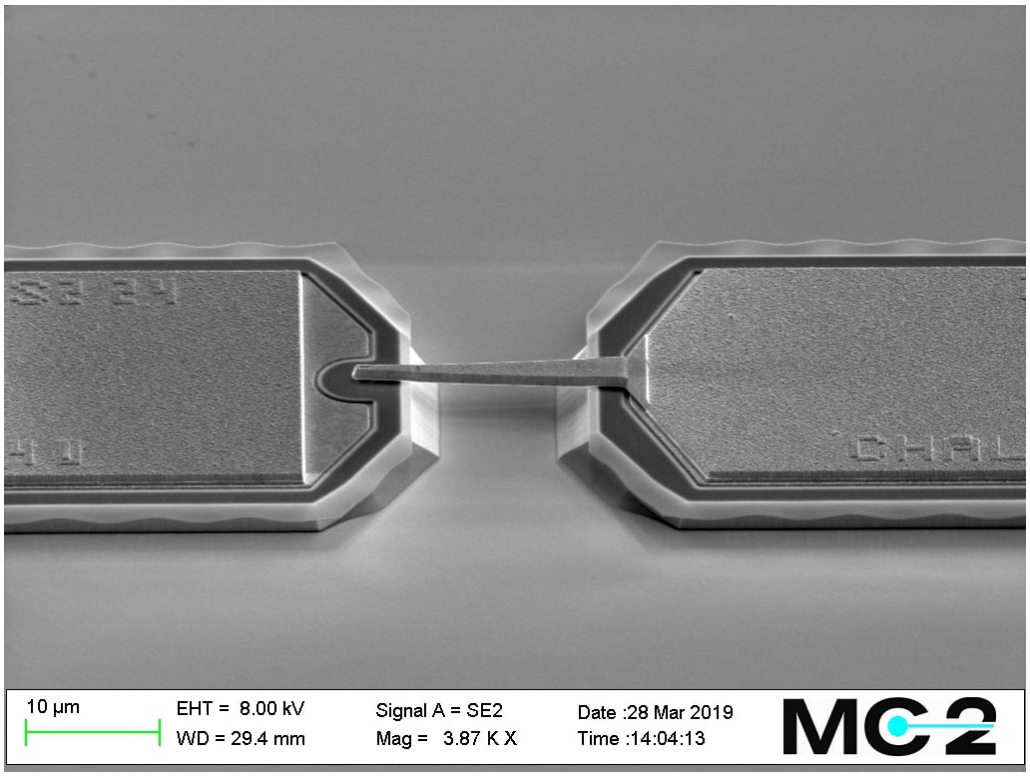

Figure 3.1: Scanned Electron Microscope picture of single-anode Schottky diode fabricated at Chalmers University of Technology

- Higher epi-layer doping concentration will eliminate plasma resonance problems [36]-[15]
- Highly doped buffer layer $5 \times 10^{18}\,\mathrm{cm}^{-3}$ on a thin GaAs membrane [5].

Based on these conclusions the harmonic mixer design was implemented in a circuit simulator using the in-built diode model. Series resistance and junction capacitance was calculated for diode contact area $0.15\,\mu\mathrm{m}^2$ and epi-layer doping concentration $5 \times 10^{17}\,\mathrm{cm}^{-3}$. Ideality factor and saturation current was set to 1.2 and 1 fA respectively. From the analytical model, series resistance was calculated by taking into of contribution from epi-layer, buffer layer, and ohmic contacts. Junction capacitance was modeled as a parallel plate capacitor and first-order fringing effects were taken into account as summarised in table 3.2.

Anode contact area	Ideality factor	Saturation current	Series resistance	Junction capacitance
$0.15\,\mu\mathrm{m}^2$	1.2	1 fA	$23\,\Omega$	0.47 fF

Table 3.2: Schottky-diode model implemented in the circuit simulator

3.5 Harmonic balance simulation

Harmonic balance is a hybrid time-frequency domain approach. The name 'Harmonic balance' stems from the idea of balancing the currents from the nonlinear

sub-circuits (via time-domain) and the currents from the linear sub-circuit in frequency domain as illustrated in figure 3.2.

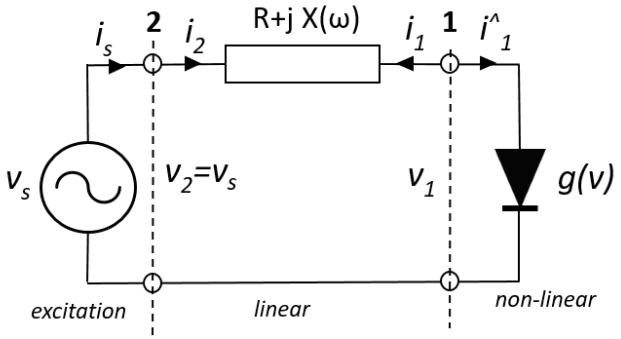

Figure 3.2: A circuit showing the linear and non-linear sub-circuits

Figure 3.3 shows the basic harmonic balance setup, Freq[1]=585 GHz is the local oscillator frequency and Freq[2]=3500 GHz is the radio frequency. Order[1] and order[2] specifies the number of harmonic frequencies that has to be calculated at the LO and RF frequencies. The optimum order for the LO frequency was found by setting a small order initially and was gradually increased until the solution had stopped changing significantly.

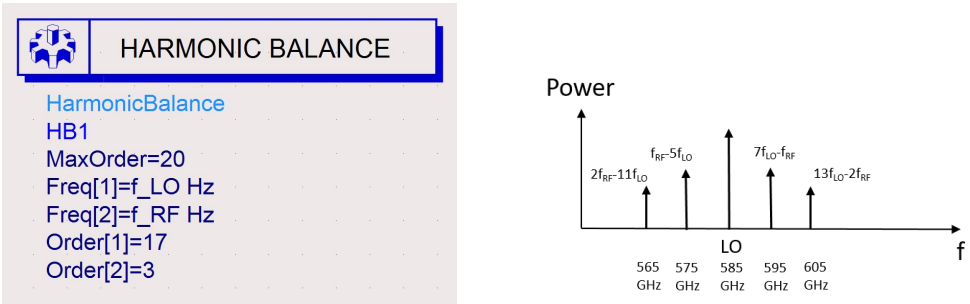

(a) **(b)**

Figure 3.3: a) Harmonic balance setup in the circuit simulator b) Double side-band inter-modulation products at LO frequency

3.6 Load pull simulation

Z_{diode} is the impedance across the Schottky diode and the complex conjugate of this impedance (Z_{diode}) is the optimum embedding impedance presented to the diode by the power source. The diode embedding impedances varies with frequency and local oscillator pump power. Therefore, it is important to find the optimum diode embedding impedances at RF, LO and IF frequencies that offers low conversion loss. Harmonic balance simulation was set up in the circuit simulator as illustrated in figure 3.4. In-order to find the optimum diode embedding impedances, load pull simulation was carried out by sweeping the RF impedance and with a fixed LO

impedance. Figure 3.5 shows the conversion loss contours from the ideal load pull simulations, with the in-built diode model with following specifications 0.15 µm^2 anode area, ideality factor of 1.2, diode series resistance equal to 23 Ω and junction capacitance of 0.47 fF. The optimum embedding RF impedance can be found at the centre of the conversion loss contours. The same procedure is followed to find the LO optimum impedance by keeping the RF impedance as constant, figure 3.6 shows the conversion loss contours in the Smith chart and the optimum LO diode embedding impedance can be found at the centre of the contours.

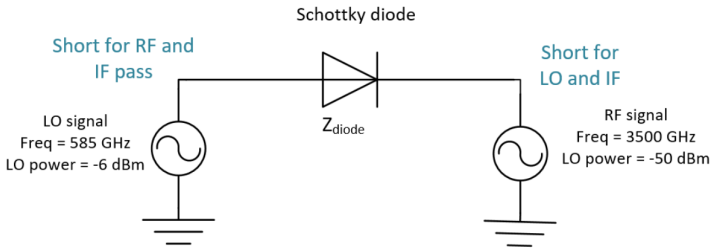

Figure 3.4: Illustration of an ideal single-ended diode mixer simulation setup.

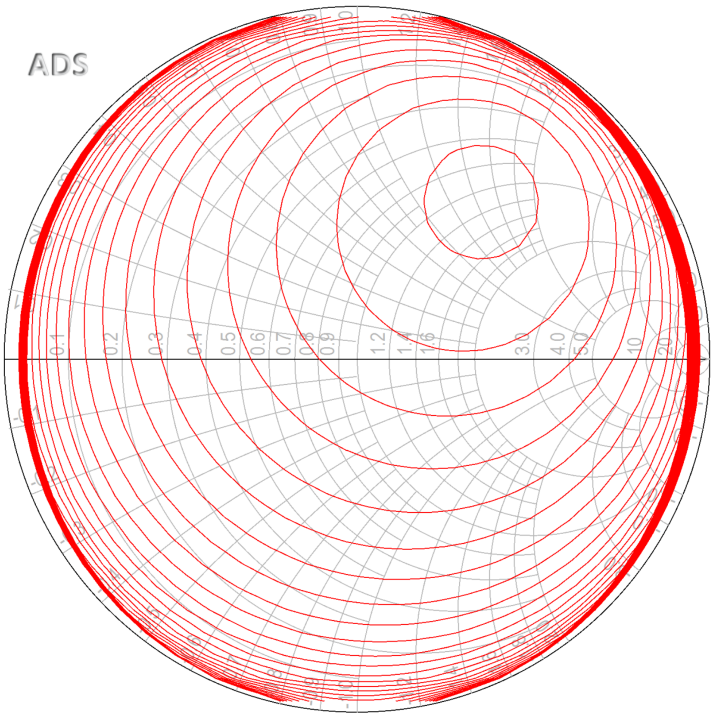

Figure 3.5: The smith chart shows the conversion loss contours from an ideal single-ended mixer simulation for −5 dBm local oscillator pump power and 1 dB step in contour. The optimum diode embedding impedance at radio frequency that yields low conversion loss is in the center of the contour.

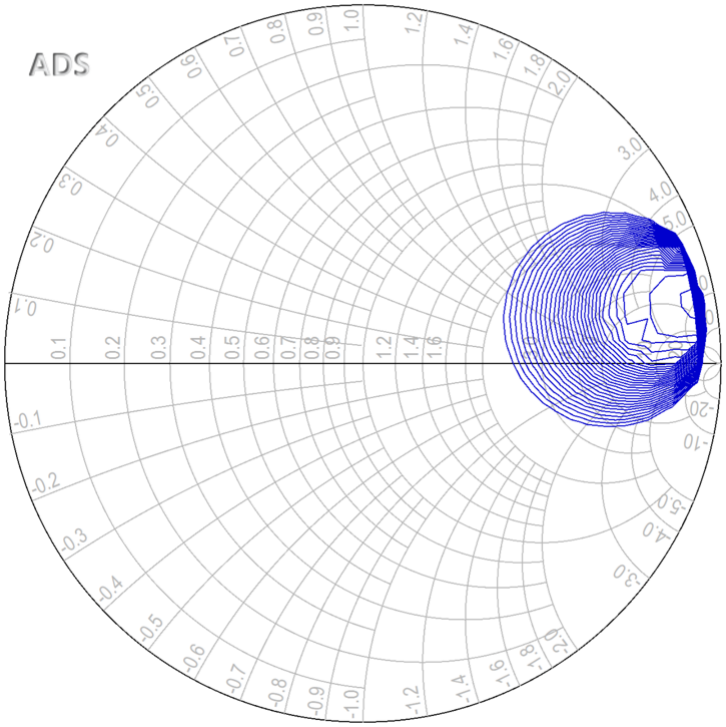

Figure 3.6: The smith chart shows the conversion loss contours from an ideal single-ended mixer simulation for −5 dBm local oscillator pump power and 3 dB step in contour. The optimum diode embedding impedance at LO frequency that yields low conversion loss is in the center of the contour.

3.7 RF and LO waveguides

Rectangular waveguides are the best option to couple energy from the fundamental TE_{10} mode to the suspended stripline mode in the channel. Almost 100% coupling can be achieved by extending the stripline into the waveguide and tuning the back-short length. The extended stripline will then act as an E-probe to couple the energy from the waveguide mode to the stripline mode. The dimensions for the RF waveguide is calculated such that the cut-off frequency is at 3 THz and also, to prevent the propagation of 5^{th} harmonic of the LO signal (2.925 THz). The aspect ratio of the waveguide was kept as 2:1 to ease the milling process. Figure 3.7a shows the 3D-EM model of 50 µm x 25 µm RF waveguide with E-plane split block (cut along H-plane symmetry line). E-plane split block offers lower loss compared to the H-plane split blocks as currents from the waveguide mode are not broken. Figure 3.7b shows the E-field distribution of the fundamental TE_{10} mode in the RF waveguide. Figure 3.7c shows the microscope picture of the RF waveguide split-block test structure milled using a 30 µm end-mill, with measured width and depth of about 28 µm. Similar to the RF waveguide, LO waveguide was designed to operate at 585 GHz, and dimension of the LO waveguide is 381 µm x 191 µm, and it

is the standard WR-1.5/WM-380 waveguide [60] and the cut-off frequency is around 400 GHz.

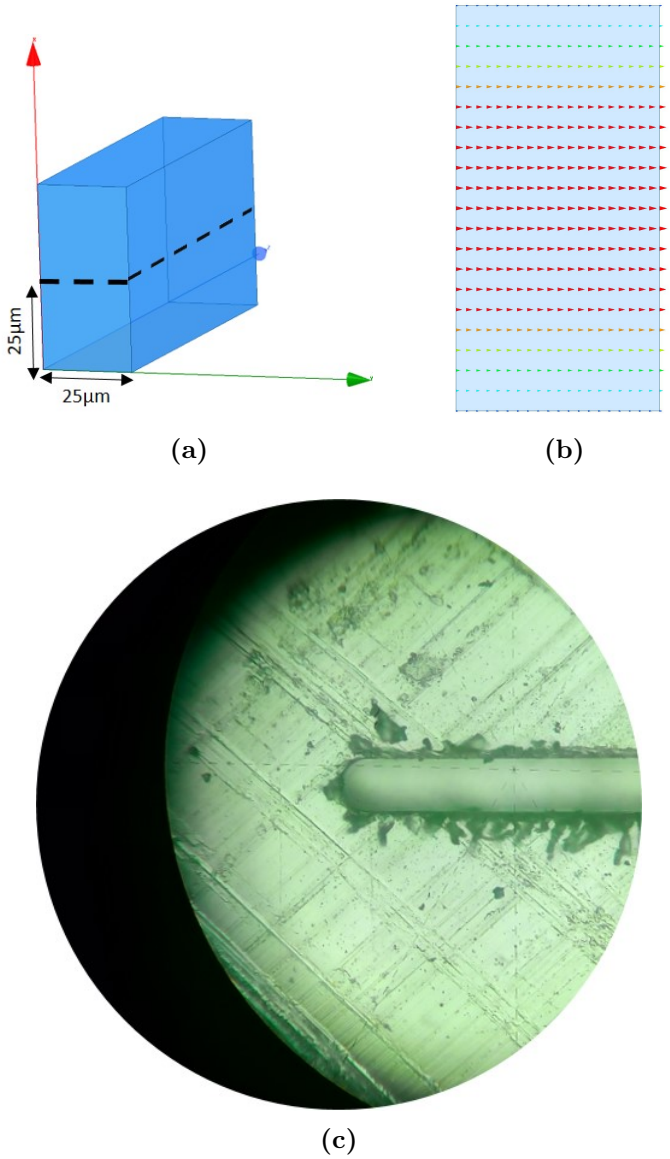

Figure 3.7: a) Picture of 3D-EM model of the RF waveguide with dotted lines showing the E-plane split block b) Electric field distribution of fundamental mode (TE_{10}) in the RF waveguide c) Picture of fabricated RF waveguide split block 28 µm x 28 µm

3.8 Planar Schottky-diode structure model

From the theoretical study described in chapter 2, the planar Schottky-diode structure was modeled in a 2 µm GaAs substrate. On top of the supporting gallium arsenide substrate, 0.5 µm thick mesa layer was defined and a thin-layer of metal and SiO_2 with 100 nm thickness was modeled as shown in figure 3.8. The Schottky

contact in the FEM simulator is modeled as a 50 Ω lumped port which is indicated by a red arrow in the figure shown below. More careful modeling of the diode structure will be carried out as a part of the future work.

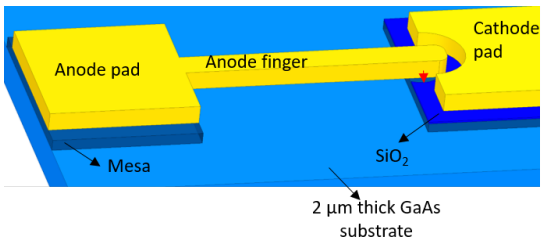

Figure 3.8: Planar Schottky diode 3D-EM model, the red arrow indicates the lumped element port defined in the FEM simulator

3.9 RF matching

In-order to have a compact, electrically small design, the RF matching was done by optimizing the diode geometry and tuning the back-short length, figure 3.9 shows the 3D electromagnetic model of the input RF waveguide and the planar Schottky diode and stepped impedance filter section which as an RF band-stop filter. Figure 3.10 shows the frequency sweep in the Smith chart and the marker indicates the impedance presented to the diode at radio frequency (3.5 THz). Figure 3.11 shows the Smith chart plot for different back-short length and the corresponding impedance presented to the diode at the radio frequency.

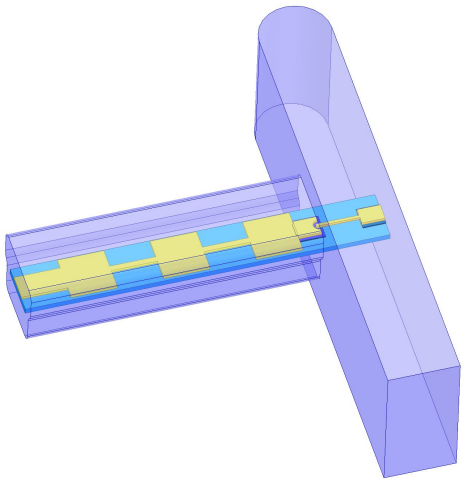

Figure 3.9: 3D electromagnetic model showing the input RF waveguide, planar Schottky diode and RF choke filter.

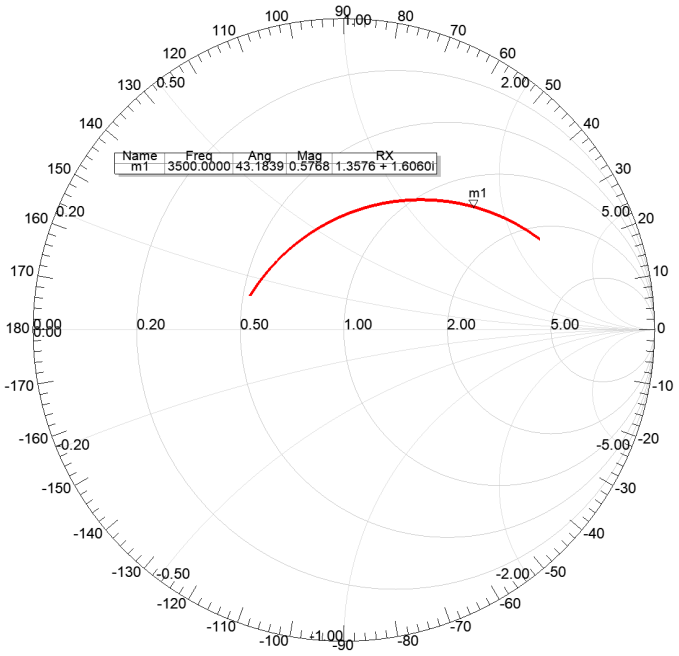

Figure 3.10: Smith chart plot with marker indicating the diode impedance at 3.5 THz

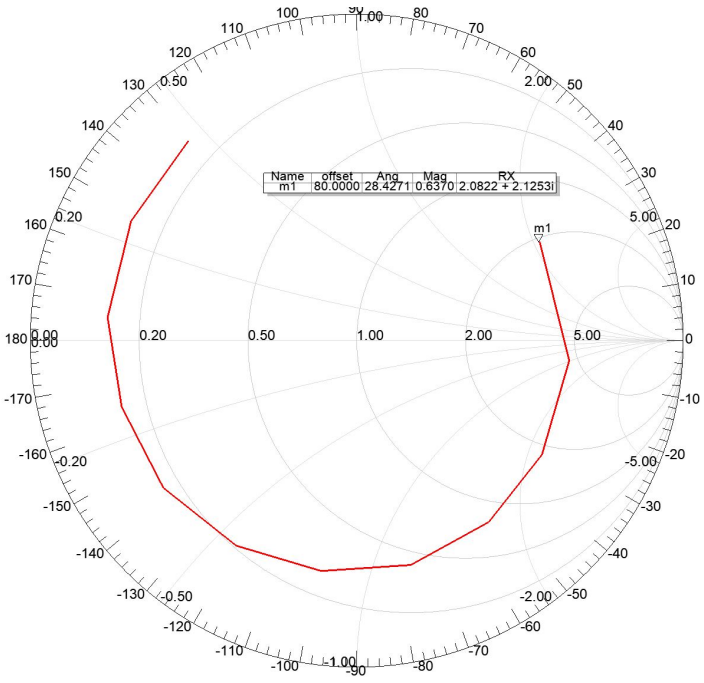

Figure 3.11: Smith chart plot showing the back-short length sweep and marker indicating the diode impedance at 3.5 THz for 80 µm back-short length

3.10 RF and LO channel

Geometry optimization of the RF channel was carried out in-order to have fundamental mode propagation up to radio frequency and prevent the existence of higher order modes. The channel is T-shaped, to reduce the uncertainity in the misalignment in the split blocks when mounted together. Figure 3.12 shows the RF-channel and the red-line indicated shows the split-block where the channel is divided into two-halves, 1 µm thick metal strip-line on 2 µm gallium arsenide substrate. Figure 3.13 shows the electric field distribution of the fundamental TEM mode, 2^{nd} order transverse mode and 3^{rd} order TE_{10} waveguide mode.The width and height of the lower and upper channel were optimized simultaneously such that only single mode propagation exists up to radio frequency. Figure 3.14 shows the electric field distribution inside the RF-channel at radio frequency.

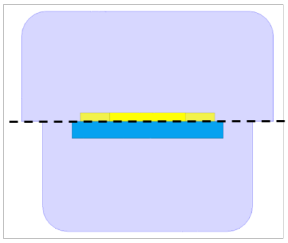

Figure 3.12: RF channel with black-line indicating the E-plane split block and suspended stripline on an ultra-thin GaAs substrate

The height of the bottom channel was kept constant (b = 13 µm) and the top channel height was swept from 12 µm to 15 µm as shown in figure 3.15. Similarly, the width of the top LO channel was swept from 250 µm to 300 µm, it is observed that for width a1 = 250 µm, single mode propagation exists up to 645 GHz as shown in figure 3.16.

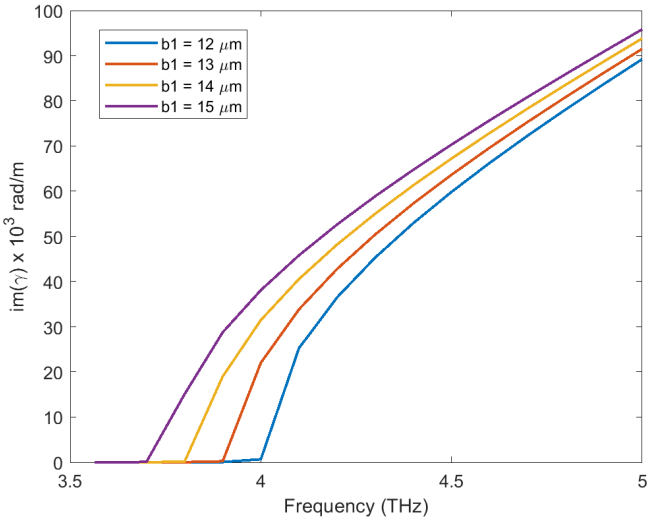

Figure 3.15: Propagation factor of the transverse (2^{nd}) mode versus frequency for different RF top channel height (b1)

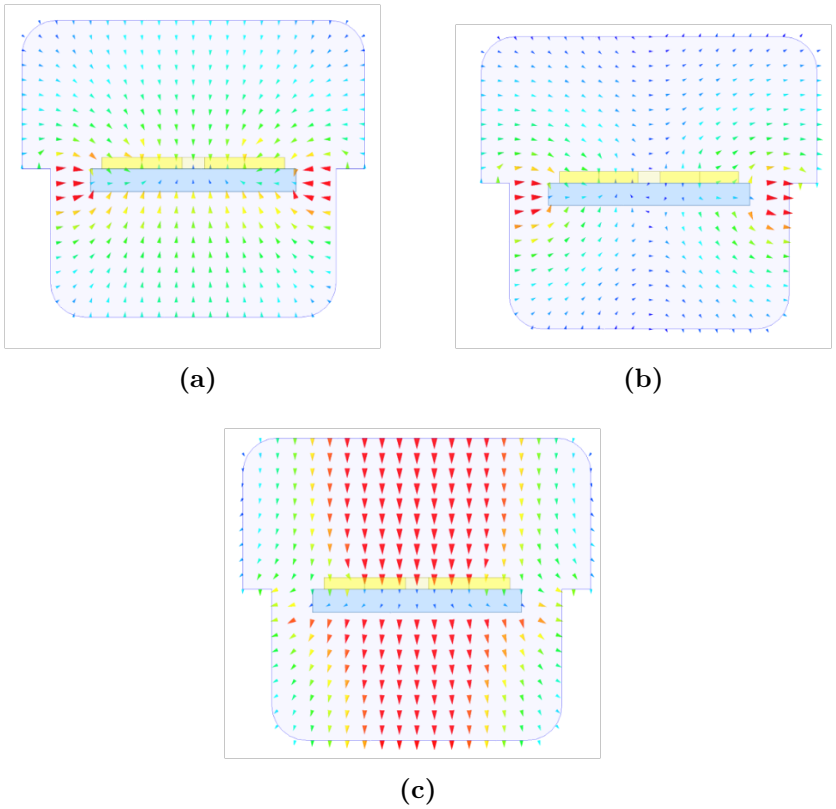

Figure 3.13: Electric field distribution in 'T-shaped' RF channel a) Fundamental mode (TEM) b) Transverse mode and c) TE_{10} mode

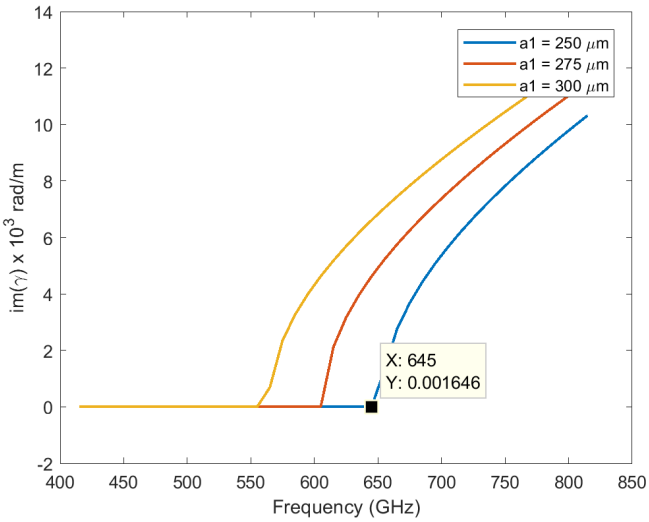

Figure 3.16: Propagation factor of the transverse (2^{nd}) mode versus frequency for different LO top channel width (a1)

Figure 3.17 shows the propagation factor plotted versus frequency for the fundamental, 2^{nd} and 3^{rd} order mode, it can be seen that there is only single-mode propagation up to 3.9 THz and the channel dimensions are 25 µm x 26 µm. The top and bot-

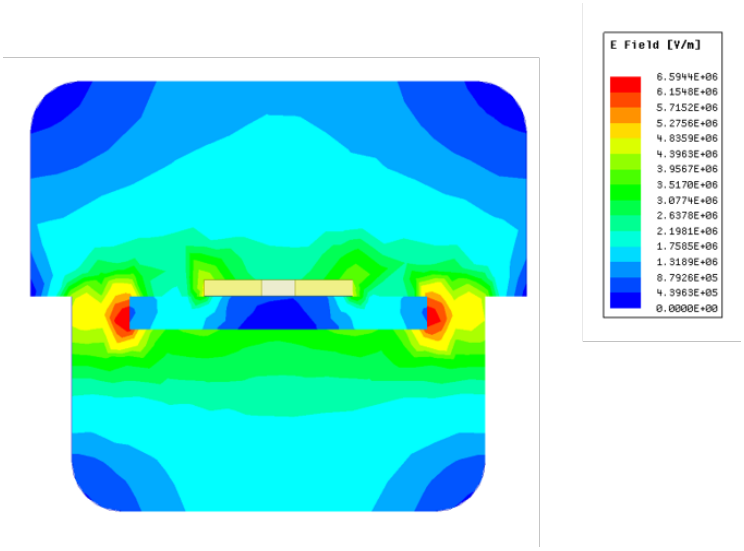

Figure 3.14: Electric field distribution in the RF-channel at 3.5 THz

tom channel dimensions were kept identical 13 µm. The same design approach was carried out, for designing the LO channel. The width, height of the bottom and top channels were optimized in-order to have fundamental mode propagation at LO frequency and also to achieve good rejection of LO signal.

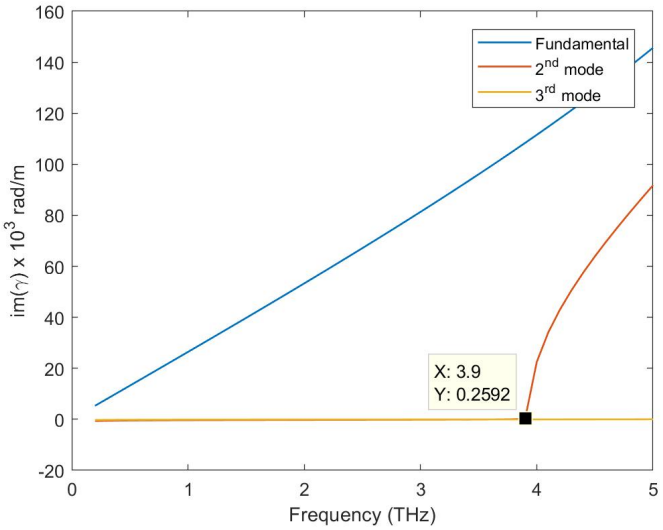

Figure 3.17: Propagation factor vs. frequency for fundamental, 2^{nd} and 3^{rd} order mode in the RF channel

Figure 3.18 shows the propagation constant versus frequency plot, it can be seen that fundamental-mode propagation exists up to 645 GHz. .

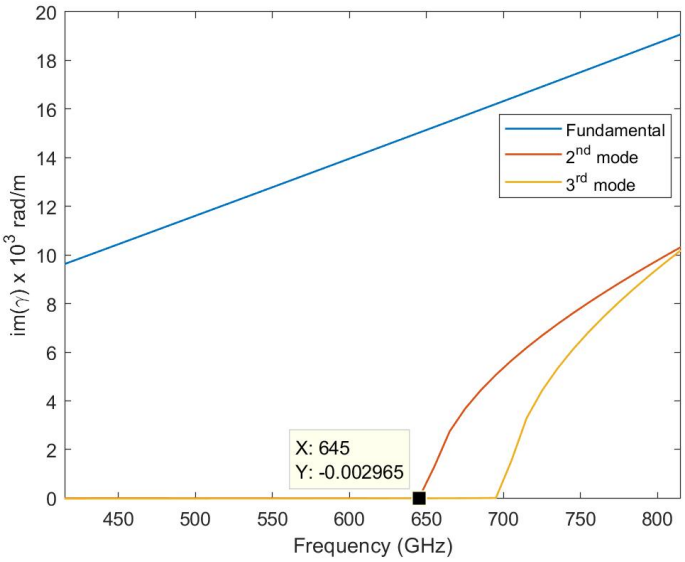

Figure 3.18: Propagation factor vs. frequency for fundamental, 2^{nd} and 3^{rd} order mode in the LO channel

3.11 Planar stepped impedance filter

3.11.1 RF choke filter

This section describes the design of a planar stepped impedance filter, that will present a short circuit ($\Gamma = -1\angle 0°$) to the RF signal and prevents it from leaking into the LO port. Initial designs were carried out in the circuit simulation software where ideal transmission lines of quarter-wave electrical length at RF frequency was implemented [39]. Figure 3.19 shows the 3D-electromagnetic model of the filter designed on a 2 µm GaAs substrate and 1 µm thick gold metal strip-line. A 5^{th} order filter design resulted in three low-impedance lines and two high-impedance lines. Thickness of the strip-line metal was varied from 0.5 µm to 1.5 µm and the corresponding filter response is as illustrated in figure 3.20. It can be observed for 0.5 µm gold thickness, the RF rejection is about −19 dB. However, it might be difficult to realise the circuit during the fabrication process.

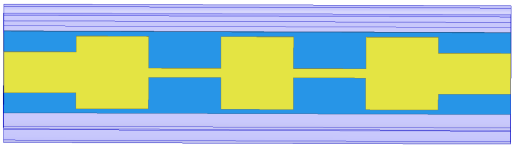

Figure 3.19: 3D-model of a 5^{th} order planar stepped impedance (RF choke filter) implemented on a 2 µm GaAs substrate

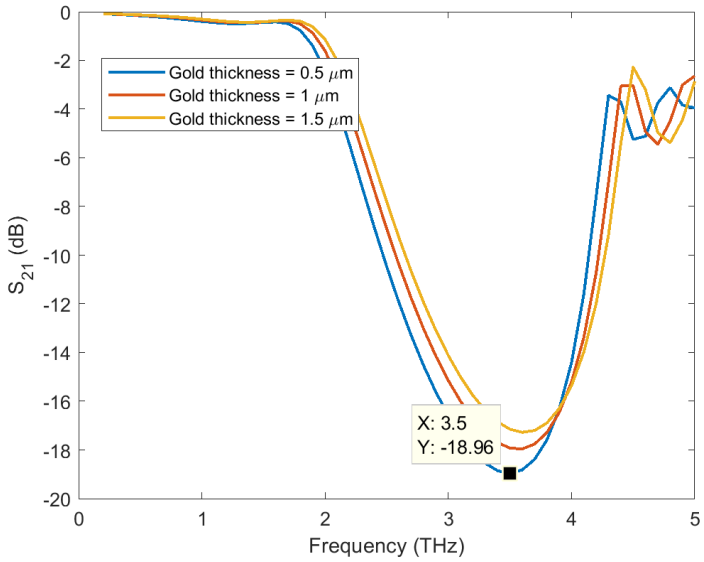

Figure 3.20: S_{21} response of the stepped impedance RF filter for different strip-line metal thickness

The electrical length of the high-low impedance lines, along with the channel dimensions were optimized to give good rejection at RF frequency, figure 3.21 shows the filter response for different electrical length of high-low impedance sections. It can be observed that the filter response is centered at 3.5 THz, when the electrical length is 16 µm. Figure figure 3.22 shows the filter response of the RF band stop filter with −18 dB rejection at radio frequency 3.5 THz.

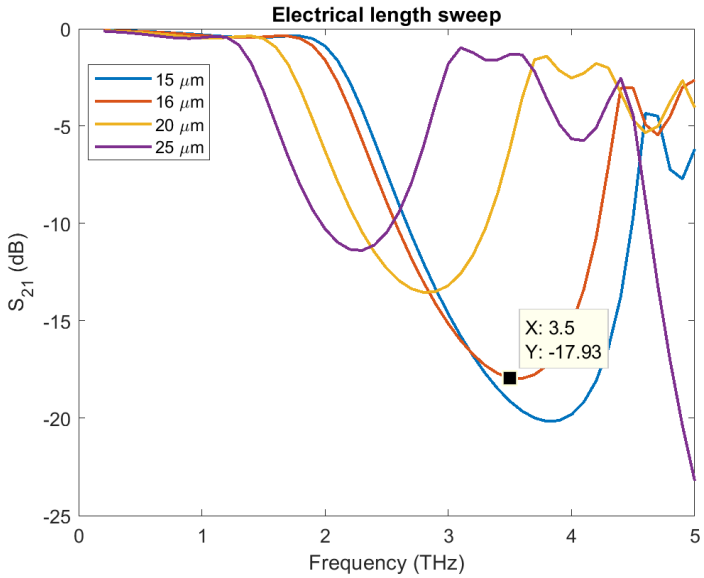

Figure 3.21: S_{21} response of the stepped impedance RF filter for different electrical length

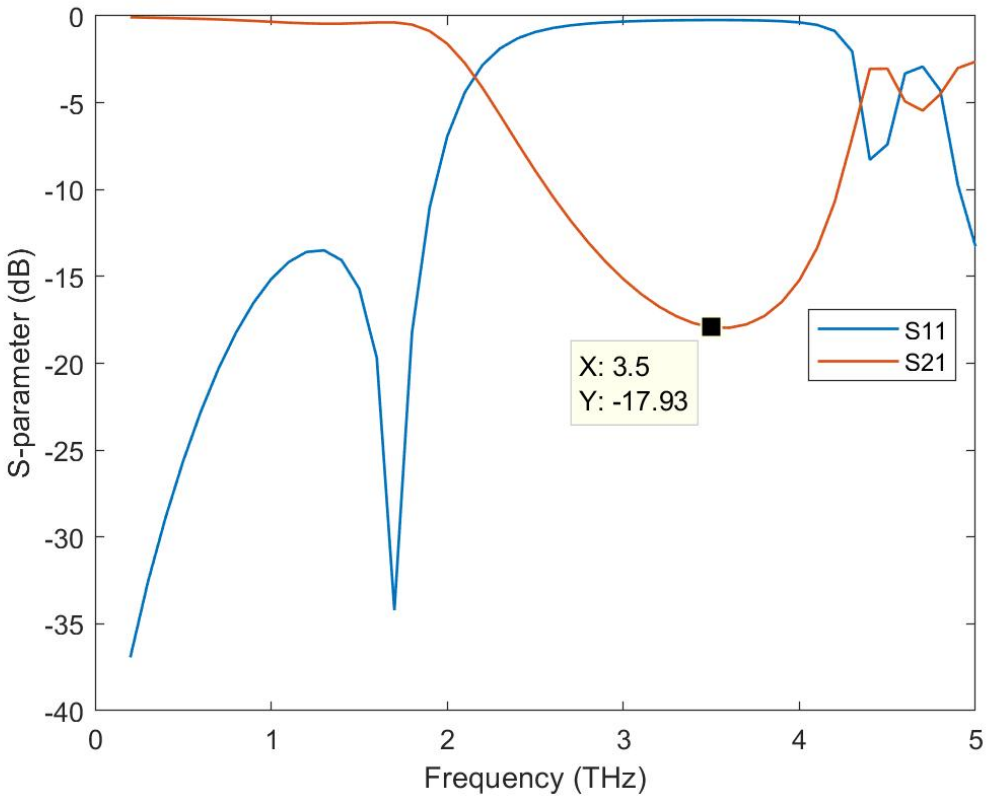

Figure 3.22: S_{11} and S_{21} response of the planar stepped impedance RF filter with -18 dB rejection at RF frequency

3.11.2 LO choke filter

To achieve good rejection at LO frequency (585 GHz) and to prevent the LO signal from leaking into the IF port, LO choke filter is designed, that will present total reflection ($\Gamma = 1$) to the LO signal. Filter was implemented with ideal transmission lines in the circuit simulator as explained in the previous section and 3D- electromagnetic model was designed in FEM software. Figure 3.23 shows the filter response of the LO choke filter for different electrical lengths. It can be observed that when the electrical length of high-low impedance lines were set to 310 µm, the filter response was centered at 585 GHz and a rejection of about -12 dB was achieved.
The height and width of top and bottom channel were also swept simultaneously in order to achieve good rejection of the local oscillator signal in to the IF chain, figure 3.24 shows the bottom channel width swept from 150 µm to 200 µm, the top channel was kept constant as 250 µm. Figure 3.25 shows the filter response from the EM simulation, at 585 GHz, rejection of about -12 dB is achieved. Beam-leads for mechanical support will be added to the LO choke filter as a part of the future work, also impedance transformer at intermediate frequencies will be included in the design.

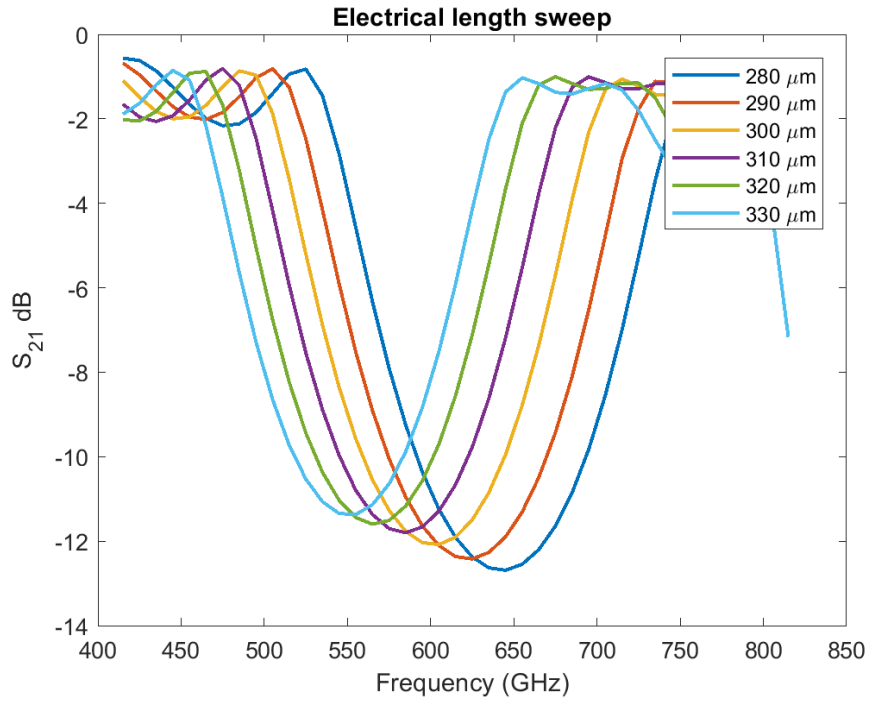

Figure 3.23: S_{21} response of the stepped impedance LO filter for different electrical length of the high-low impedance sections.

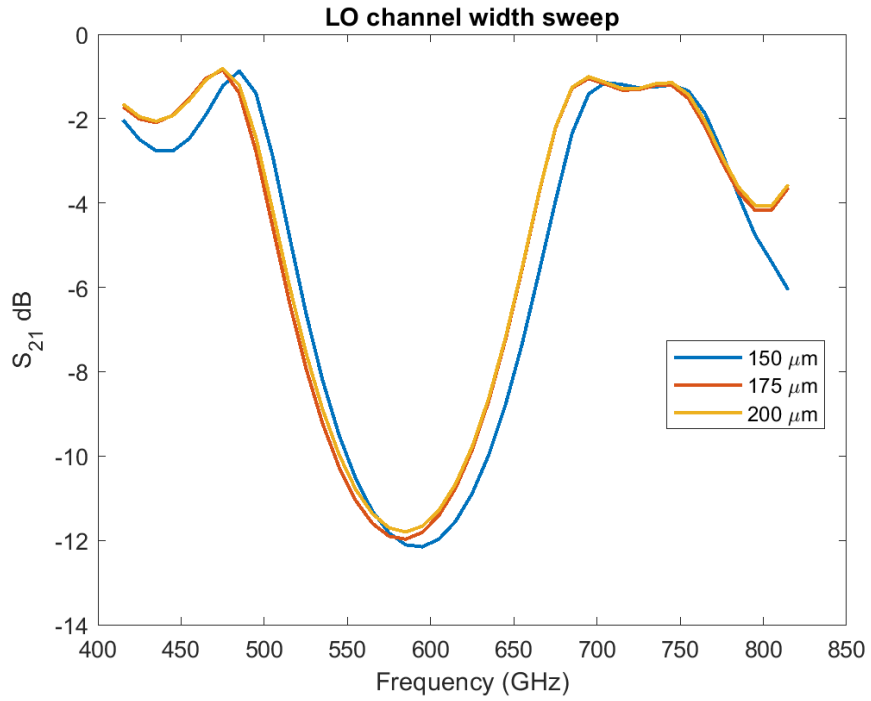

Figure 3.24: S_{21} response of the stepped impedance filter for different bottom channel width.

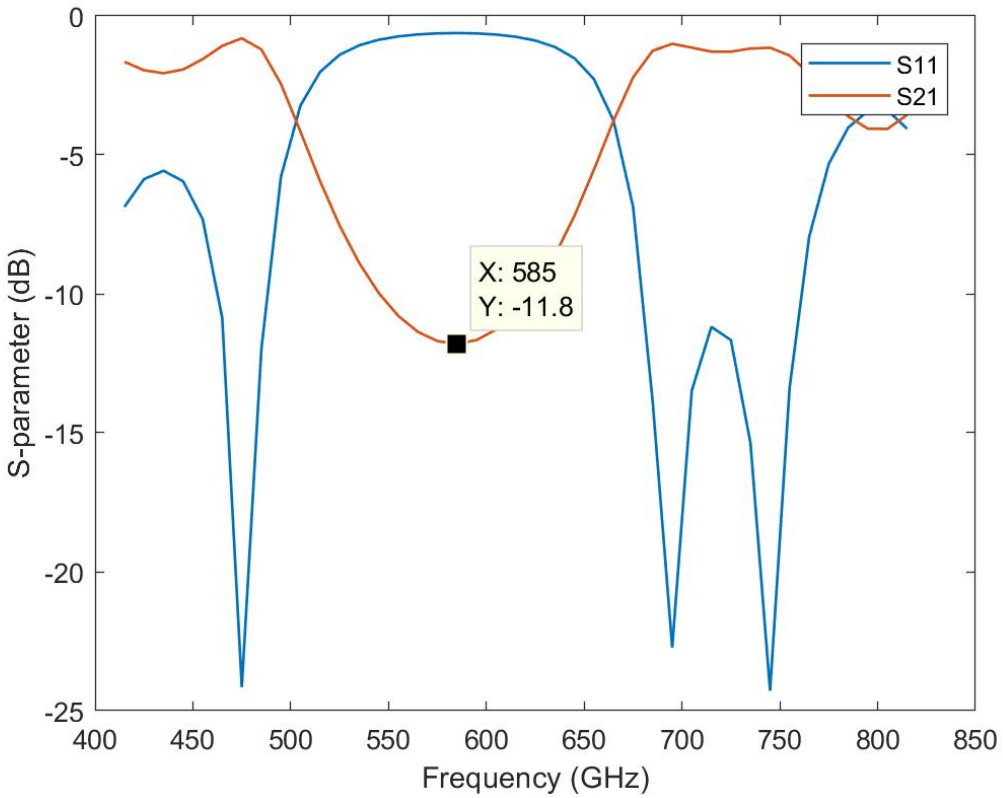

Figure 3.25: S_{11} and S_{21} response of the stepped impedance filter with -12 dB rejection at LO frequency

3.12 LO matching

The LO waveguide was designed with reduced waveguide height (380 µm x 95 µm) as shown in figure 3.26. The de-embedding distance of the waveguide as indicated by blue arrow in the figure shown below was varied. The LO back-short length, LO probe width was varied in-order to present the desired impedance at LO frequency. The full port impedance of the lumped port that models the Schottky contact is the complex conjugate of the optimum embedding diode impedance at LO frequency 585 GHz which is approximately equal to 150-j*300 Ω. Figure 3.27 shows the Smith chart with a marker indicating the impedance presented to the diode at LO frequency.

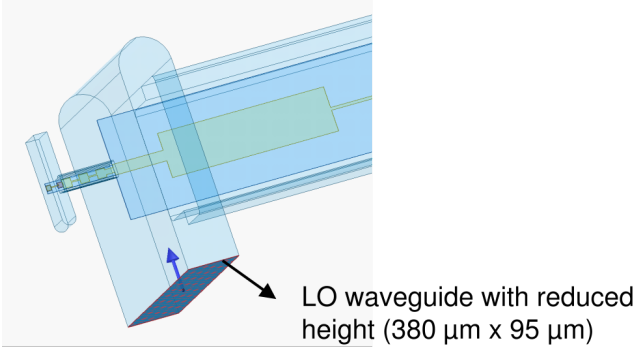

Figure 3.26: 3D electromagnetic model of x6 harmonic mixer with reduced LO waveguide height and blue arrow shows the de-embedding distance into the LO waveguide.

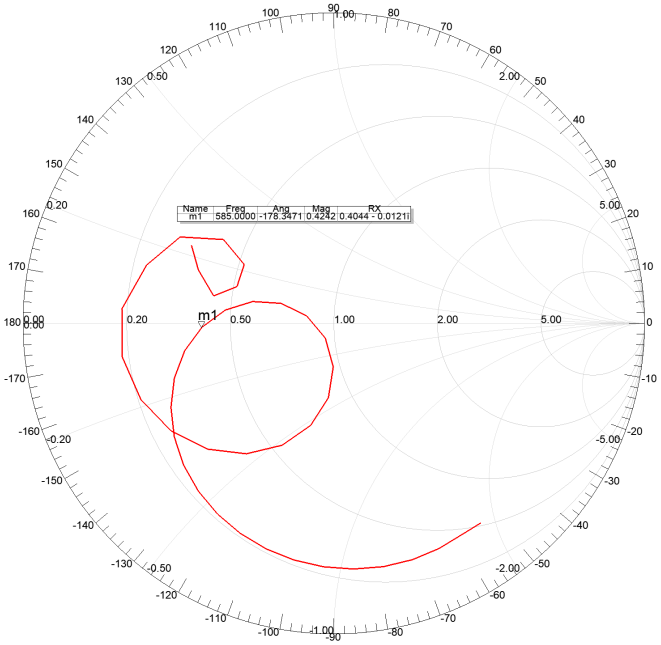

Figure 3.27: Smith chart showing the impedance at LO frequency 585 GHz

A quarter wave waveguide transformer as shown in figure 3.28 was designed in-order to present the optimum diode embedding impedance at LO frequency. Geometry of the quarter-wave waveguide transformer wave optimized in-order to match LO waveguide impedance to the optimum diode embedding impedance at LO frequency. Figure 3.29 shows the impedance presented to the diode at LO frequency, fractional bandwidth of about 7% was achieved.

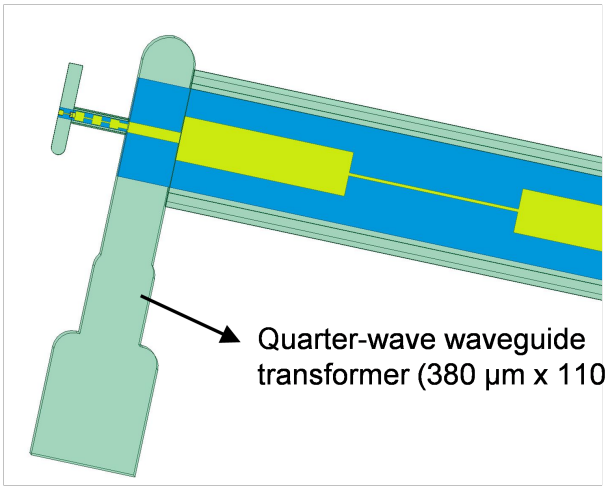

Figure 3.28: Model showing the quarter-wave waveguide impedance transformer

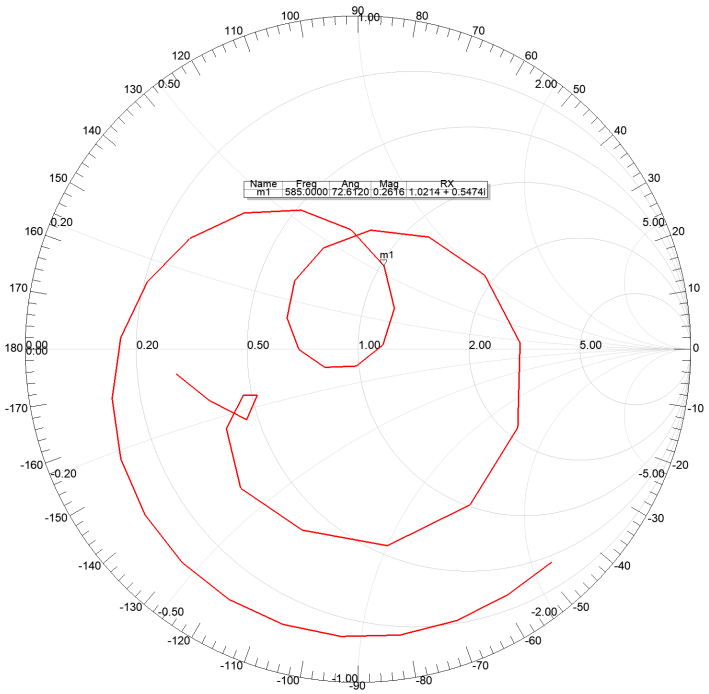

Figure 3.29: Smith chart with frequency sweep and maker indicates the impedance presented to the diode at LO frequency.

4

Results

This chapter presents the results from ideal mixer simulation. The mixer performance and optimum embedding impedances at LO, RF, and intermediate frequencies are presented for Z-, and Y-mixer configurations. A full 3D electromagnetic model of the x6 harmonic mixer is presented, S-parameters from the EM model were then exported to the circuit simulator to evaluate the overall performance of the circuit in terms of conversion loss. This process was carried out in an iterative manner until good performance was achieved.

4.1 Diode model parameter extraction

Based on the series resistance (R_s) and the junction capacitance value (C_j) obtained from the analytical model for a given anode area, DC simulation was setup in the circuit simulator [61]. Figure 4.1 shows the I-V plot of the diode model with $R_s = 23\,\Omega$, $\eta = 1.2$, $C_j = 0.47\,\text{fF}$, $I_{sat} = 1\,\text{fA}$ and $N_{d,epi} = 5 \times 10^{17}\,\text{cm}^{-3}$ for $0.15\,\mu\text{m}^2$ anode area and measurement performed with Kelvin probes at room temperature in dark condition.

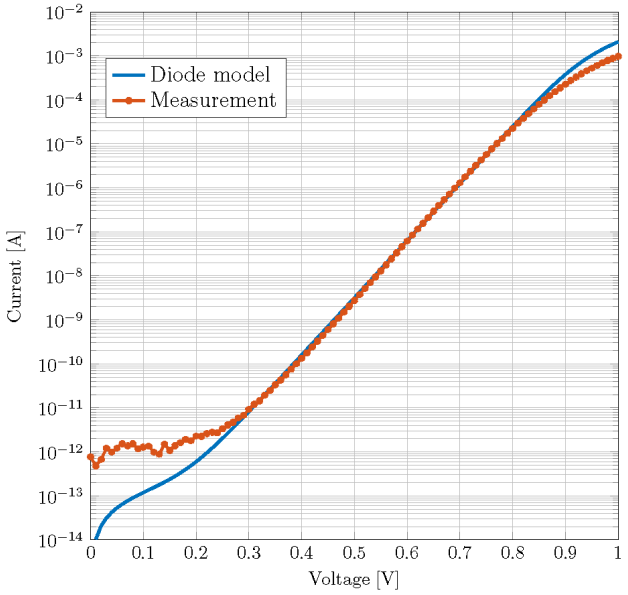

Figure 4.1: In-built diode model from the circuit simulator and measurement data of in-house Schottky diode with $0.15\,\mu\text{m}^2$ anode area

4.2 Comparison of analytical diode series resistance model with FEM simulation

In-order to verify this analytical model, single anode diode structure was designed in finite element method simulation software. Thickness of the epi-layer region was calculated from the zero-bias depletion width which was approximately equal to 50 nm and the electrical conductivity of the epi-layer region was calculated for $5 \times 10^{18}\,\mathrm{cm}^{-3}$ doping concentration. Area of the anode contact was varied and the corresponding resistance was calculated and compared to the analytical model as shown in figure 4.2. Self heating and high-frequency effects are excluded in this analytical model [62], [63].

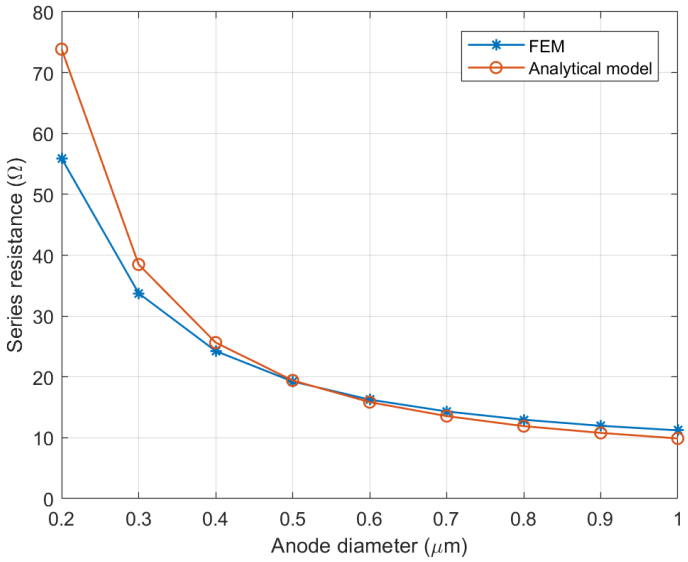

Figure 4.2: Comparison of dc-series resistance of analytical model with FEM simulation for different anode contact area

4.3 Optimum mixer configuration

Four basic topologies: Z-,Y-,H-,G- mixers were implemented in the circuit simulation software, embedding impedances at RF, LO and IF frequencies were optimised such that minimum conversion loss is achieved. The out-of-band frequencies were divided in two groups: odd and even-order frequencies and they were terminated reactively either by a short or open circuit. At high frequencies, junction capacitance will present a short circuit therefore it is not a pure Z-mixer [64]. The local oscillator pump power was varied from −20 dBm to −3 dBm. It is also crucial to note that the voltage swing does not exceed above 1 V. The ideal-mixer simulations of Z- ,Y- mixer topologies were carried out, where the out-of-band frequencies are either open or short circuited respectively. Conversion loss versus LO pump power was plotted for three different harmonic mixers: x4, x6, and x8 operating at 2.3 THz,

3.5 THz, and 4.7 THz respectively, 585 GHz LO frequency and 10 GHz intermediate frequency. Figure 4.3 shows the conversion nulls observed in Y-mixers due to the destructive interference caused by multiple mixing products [65].

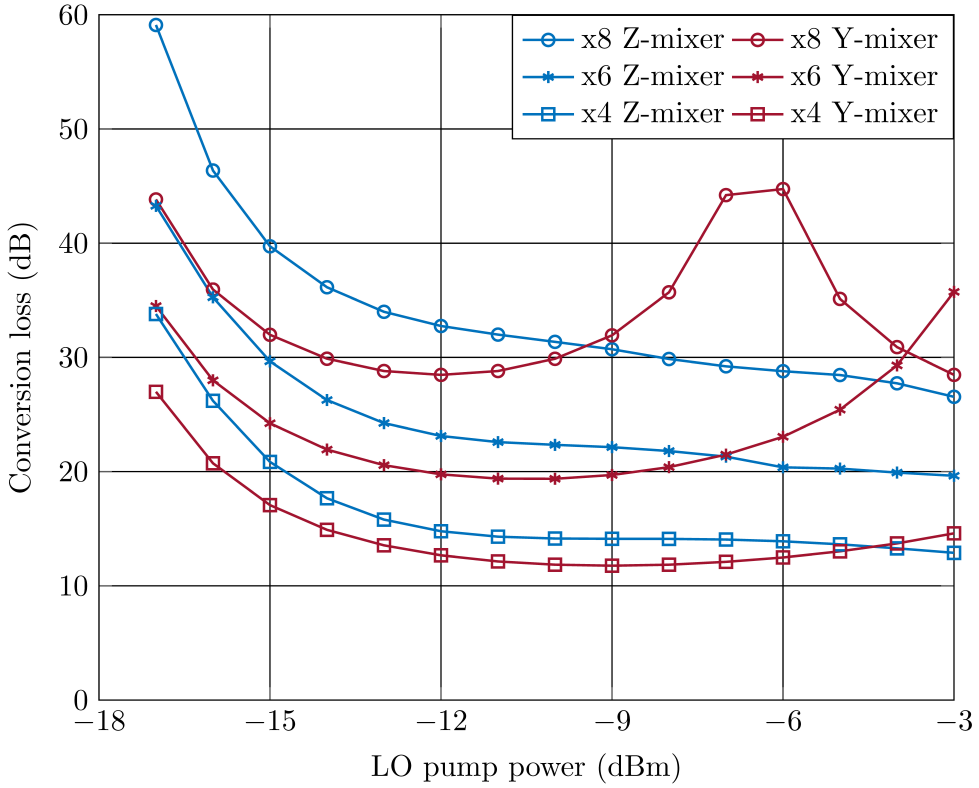

Figure 4.3: Conversion loss versus LO pump power of Z-, and Y-mixer topology for x4, x6, and x8 harmonic mixers operating at 2.3 THz, 3.5 THz, and 4.7 THz respectively

Table 4.1 summarises the minimum conversion that can be obtained for various mixer configurations for different diode series resistance. Detailed large-signal analysis of four basic mixer configurations: Y-, Z-, H-, G-mixers shows that the Y-mixer has low conversion loss at low LO power. However, Z-mixer provides the least conversion loss, as the pump power increases due to associated power dissipation in the idler-circuits.

Mixer topology	CL (dB) $R_s = 25\Omega$	CL (dB) $R_S = 50\Omega$	CL (dB) $R_S = 100\Omega$
Z-mixer	20.8	24.4	28.3
H-mixer	23.9	31.9	35.4
Y-mixer	23.1	32.9	36.1
G-mixer	25.2	33.8	39.9

Table 4.1: Minimum conversion loss for four basic mixer configuration: Z-, Y-, H-, and G-mixers for different diode series resistance.

Time-domain voltage versus current is plotted for the ideal circuit simulation for different local oscillator pump power as shown in figure 4.4. For low local oscillator

pump power, the reactive part dominates (capacitive current) and as the pump power increases, the resistive contribution increases in the forward bias region.

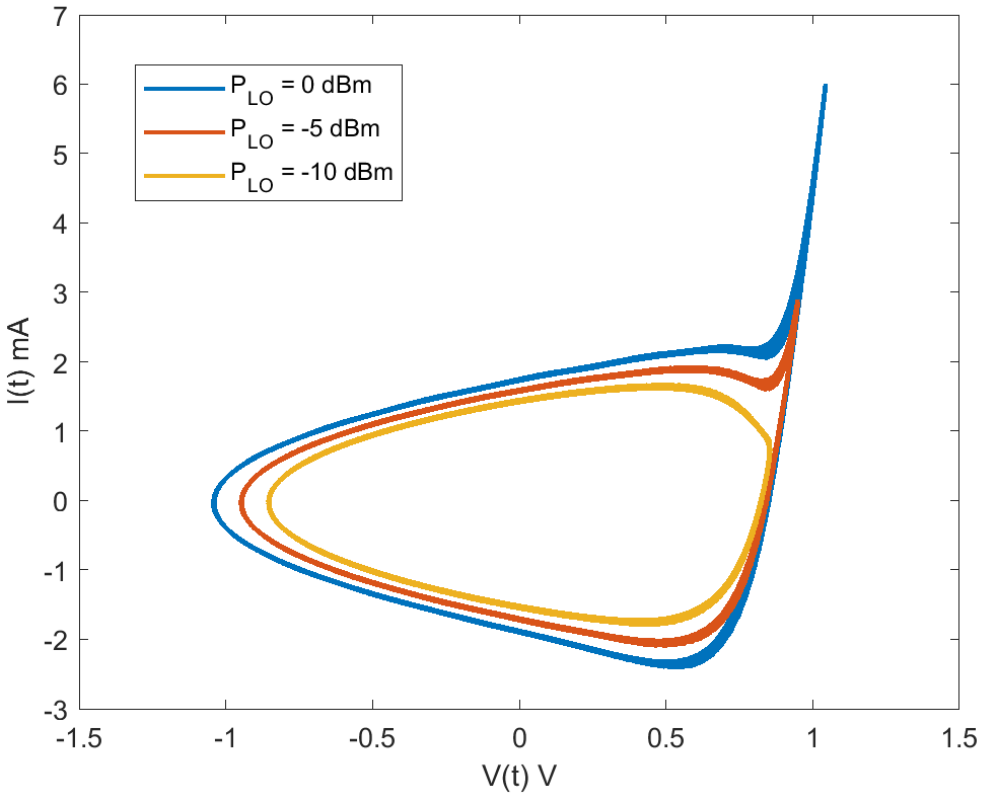

Figure 4.4: Comparison of time domain voltage versus current for ideal circuit simulation and different local oscillator pump power

4.4 Optimum embedding impedances

Optimum embedding impedances at RF, LO and intermediate frequencies for Y-mixer configuration in which all out-of-band frequencies are terminated with a short circuit are illustrated in figure 4.5. It can be observed from the following figure, for a given local oscillator pump power, when the diode series resistance was varied, the optimum embedding impedance that offers least conversion loss varies correspondingly. The optimum embedding impedance at radio frequency is sensitive to the variation in diode series resistance whereas, the optimum embedding impedance at local oscillator frequency does not vary much when the diode series resistance is varied. Optimum embedding impedance at intermediate frequency varies along the real axis of the smith chart and increases as the diode series resistance increases.

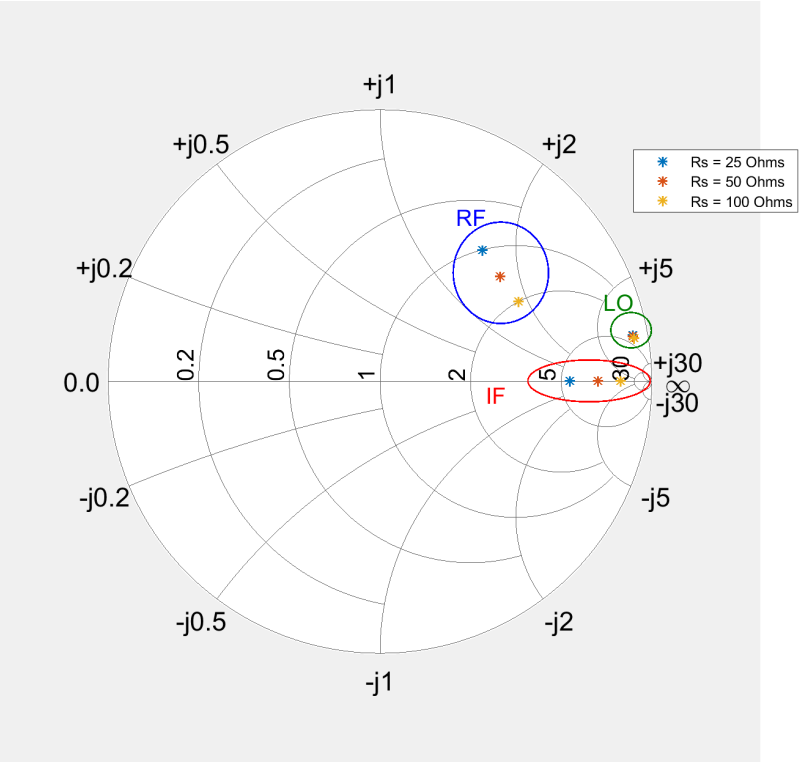

Figure 4.5: Normalised optimum embedding impedances presented for single-ended diode Y-mixer at RF, LO and Intermediate frequencies for different diode series resistance R_s for $-6\,\text{dBm}$ local oscillator pump power and $P_{RF} = -50\,\text{dBm}$

Figure 4.6 and 4.8 shows the optimum LO and RF embedding impedance plotted in the impedance (Z)-plane for x4, x6, and x8 harmonic mixers for two mixer configurations: Y- and Z-mixers in which the out-of-band frequencies are terminated with a short and open circuit respectively. At low LO power, the optimum embedding impedance is equal to the small-signal impedance of the diode-equivalent circuit $(R_s + C_{j0})$. The optimum embedding impedances are calculated by optimizing the impedances at RF, LO, and IF frequencies to obtain least conversion loss. The LO pump power was varied from $-20\,\text{dBm}$ to $-3\,\text{dBm}$, and the arrow indicates the direction of increasing LO power. X-axis of the Z-plane is normalised to the series resistance of the diode ($R_s = 23\Omega$) and the Y-axis is normalised to the zero-bias junction capacitance ($C_{j0} = 0.47fF$). Real part of the RF and LO optimum embedding impedance is plotted versus LO pump power for x4, x6 and x8 harmonic mixers in Z-, Y- mixer configuration as shown in figure 4.7-4.9 respectively. It is evident from the figures that at low LO operating power, the real part of the optimum embedding impedance is approximately equal to the the series resistance of the diode (R_s). Figure 4.10-4.11 presents the optimum embedding impedances at RF and LO frequencies in a smith chart for different local oscillator pump power for Y-mixer configuration. Optimum embedding impedance at intermediate frequency for x4, x6 and x8 harmonic mixers for Y-mixer topology is presented in the impedance plane in figure 4.12.

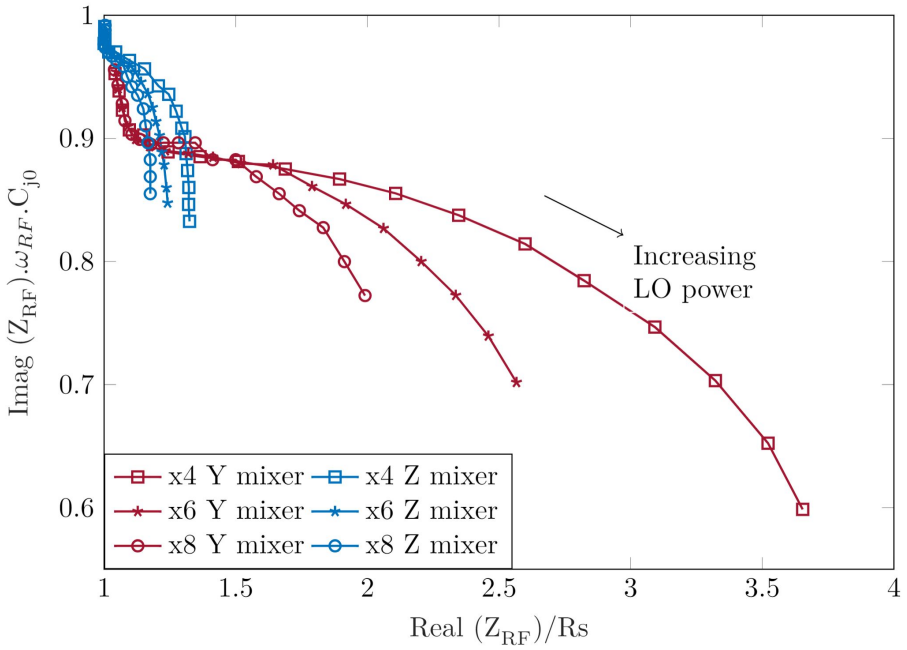

Figure 4.6: Normalised optimum RF embedding impedance at 3.5 THz plotted for x4, x6, and x8 harmonic mixers in Z-, and Y-mixer configuration in Z-plane for LO power sweep from −20 dBm to −3 dBm, where $R_s = 23\,\Omega$ is the diode series resistance and $C_{j0} = 0.47\,\text{fF}$ is the zero-bias junction capacitance and n is the harmonic index

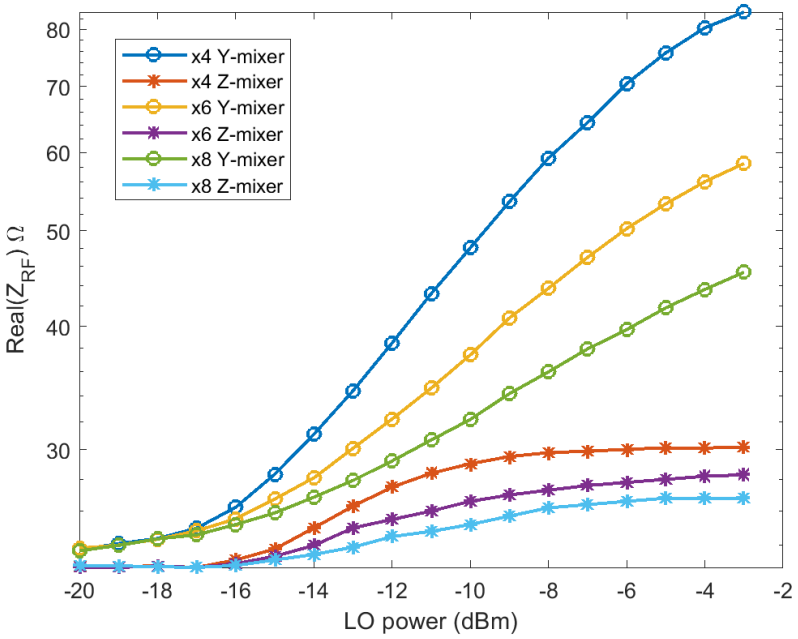

Figure 4.7: Real part of RF optimum embedding impedances versus LO pump power for x4, x6, and x8 harmonic mixers in Z-, and Y-mixer configuration.

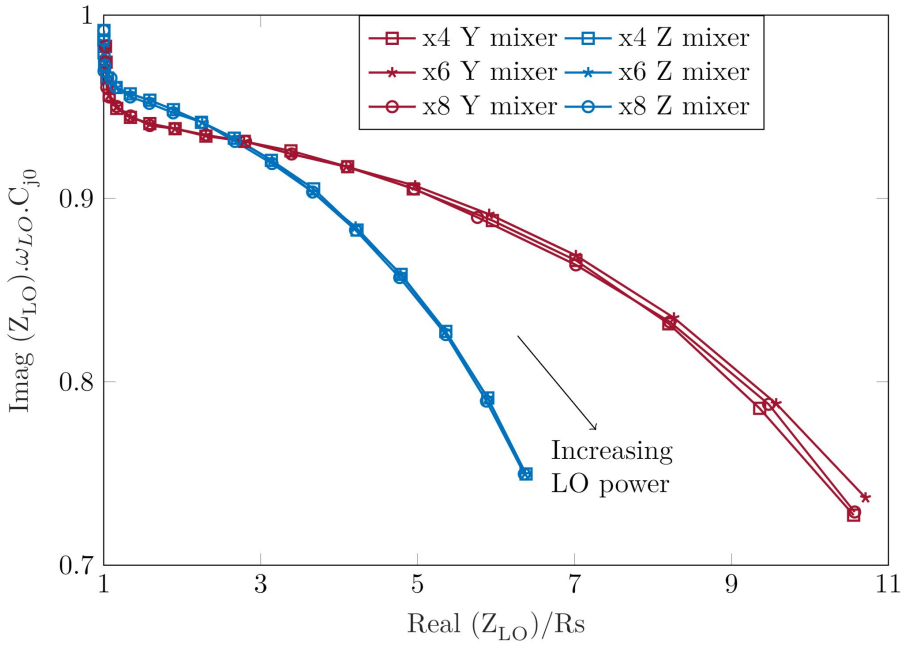

Figure 4.8: Normalised optimum LO embedding impedance at 585 GHz plotted for x4, x6, and x8 harmonic mixers in Z-, and Y-mixer configuration in Z-plane for LO power sweep from −20 dBm to −3 dBm, where $R_s = 23\,\Omega$ is the diode series resistance and $C_{j0} = 0.47$ fF is the zero-bias junction capacitance and n is the harmonic index

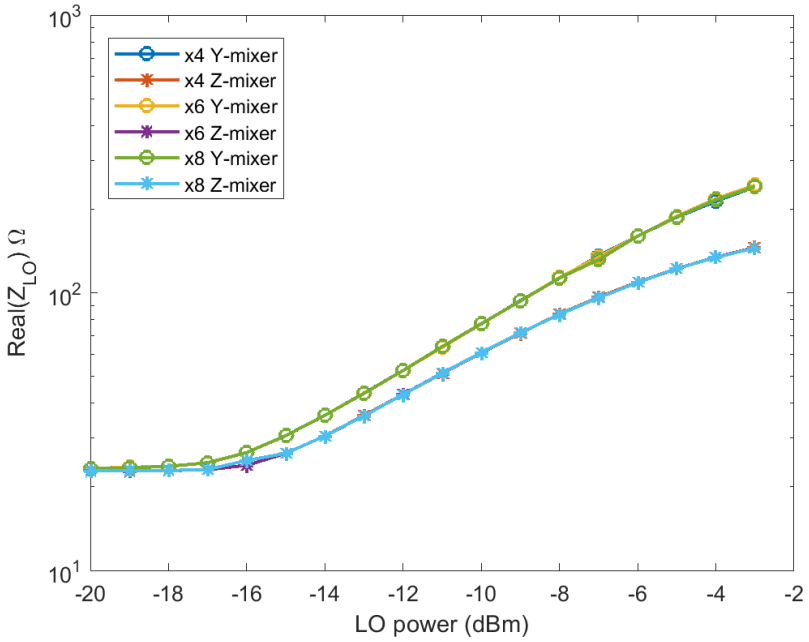

Figure 4.9: Real part of LO optimum embedding impedances versus LO pump power for x4, x6, and x8 harmonic mixers in Z-, and Y-mixer configuration.

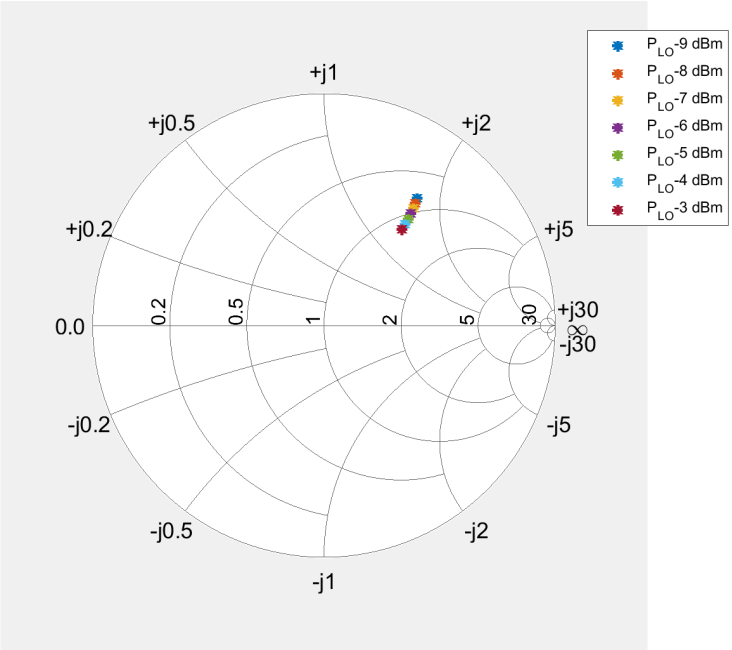

Figure 4.10: Smith chart showing the optimum embedding impedances at radio frequency (3.5 THz) for different local oscillator pump power for Y-mixer configuration.

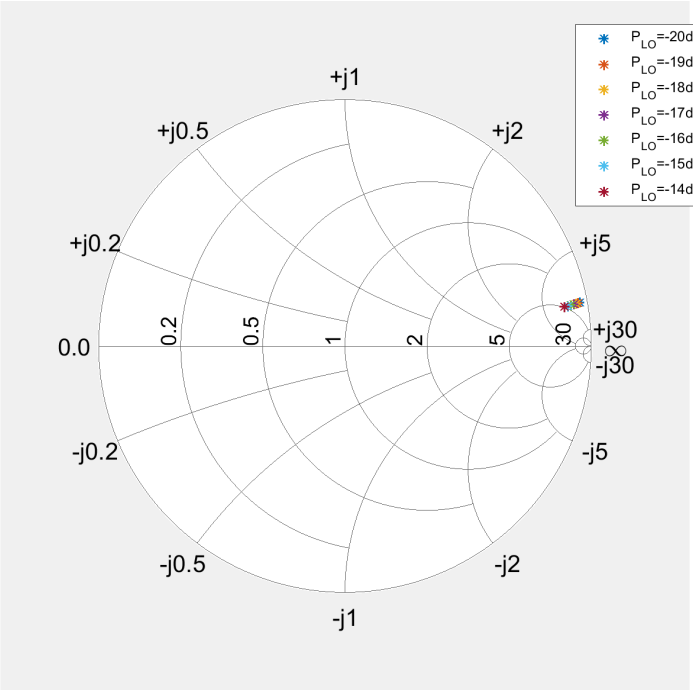

Figure 4.11: Smith chart showing the optimum embedding impedances at local oscillator frequency (585 GHz) for different local oscillator pump power for Y-mixer configuration.

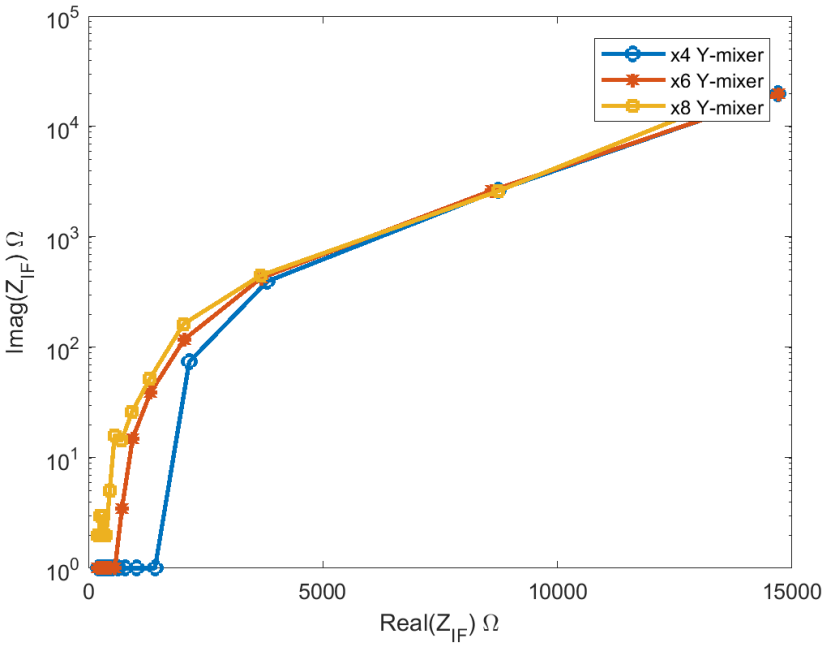

Figure 4.12: Optimum embedding impedances at intermediate frequency presented for single-ended diode x4, x6, and x8 harmonic mixer in Y-mixer configuration.

4.5 Design of x6 harmonic mixer

Each sub-block were designed and optimised separately till the design goals were achieved. Later, the sub-blocks were put together and optimised again. Figure 4.13 shows the 3D-electromagnetic model of x6 harmonic mixer operating at 3.5 THz. RF and LO band-stop filter has 5^{th} order high-low impedance lines, which prevents RF signal from leaking into the LO chain and LO signal from leaking into the IF chain respectively. Geometry of Schottky-diode and back-short distance is varied such that the RF optimum impedance is presented to the diode at RF frequency (3.5 THz). In-order to present the optimum LO impedance at LO frequency (585 GHz). LO waveguide with reduced height was designed, length and height of the quarter-wave section impedance transformer is varied to present optimum LO impedance to the diode and also achieve broad-band frequency response.

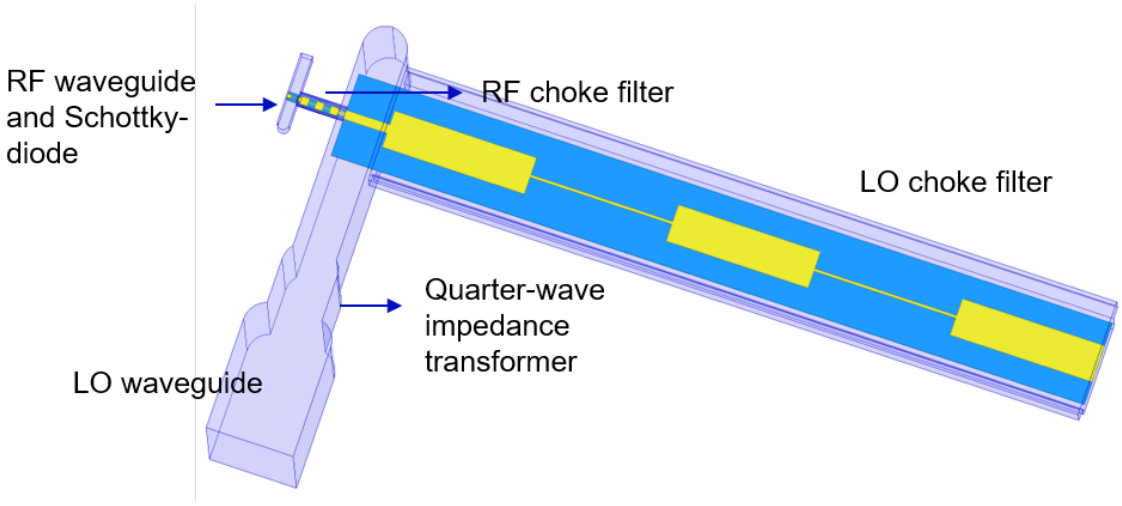

Figure 4.13: 3D-Electromagnetic model of 3.5 THz Schottky-based harmonic mixer showing the RF waveguide, Schottky diode, RF band-stop filter, LO waveguide operating at 585 GHz and LO choke filter.

4.5.1 Initial mixer simulation

S-parameters from the full 3D-electromagnetic model was exported to the circuit simulator. The intermediate frequency port was terminated with 300Ω impedance and the local oscillator pump power was swept from −6 dBm to −3 dBm and conversion loss is plotted as shown in figure 4.14. The pump power was swept till −3 dBm as the voltage swing should not exceed +1 V. This simulation does not include additional losses due to metal waveguide (PEC boundary), only losses in the gold stripline was taken into account. Figure 4.14 shows the comparison of two simulations with perfect conductivity and finite conductivity boundary condition.

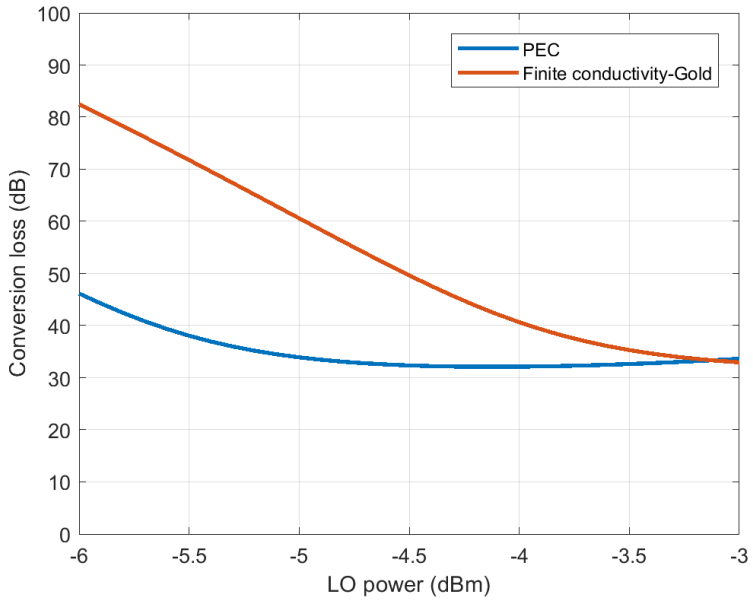

Figure 4.14: Conversion loss versus local oscillator pump power sweep for perfect electric conductor (PEC) and finite conductivity boundary conditions. IF port was terminated with 300Ω impedance in the circuit simulator. Conversion loss of about 34 dB was obtained for −5 dBm of LO pump power for PEC boundary which takes into account of losses in the stripline.

Figure 4.15 shows comparison of PEC and finite conductivity boundary for RF frequency sweep from 3.48 THz to 3.52 THz for Schottky diode model with $R_s = 23\Omega$, $C_{j0} = 0.47fF$. Figure 4.16 shows comparison conversion loss versus LO power sweep for ideal R_s and for higher series resistances. It can be observed that for lower LO power, conversion loss gets worse as the diode series resistance increases due to the variation in optimum embedding impedances. However, as the pump power increases, the conversion efficiency improves. For ideal R_s, conversion loss is about 32 dB, for $R_s = 50\Omega$ conversion loss is 35 dBm, for −4 dBm LO pump power. Figure 4.17 shows the electric field distribution in the full-mixer circuit in the LO frequency (585 GHz).

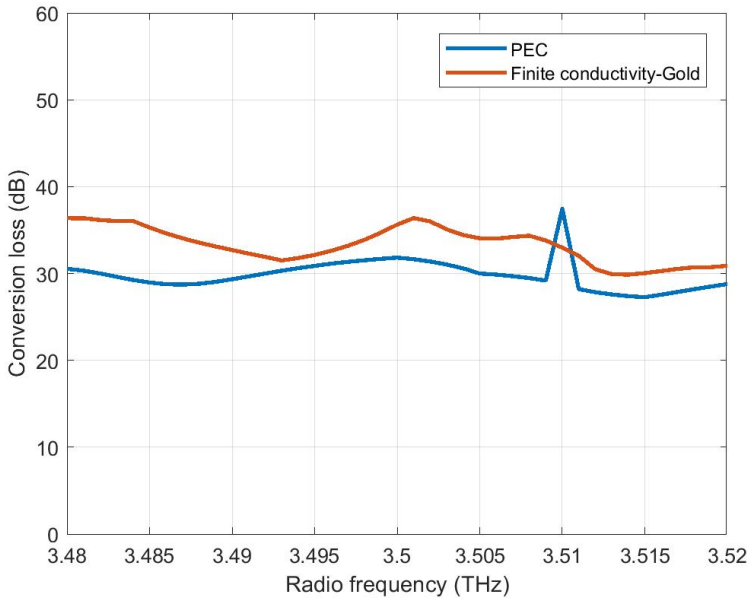

Figure 4.15: Conversion loss versus radio frequency sweep for LO frequency = 585 GHz, P_{LO} = -4 dBm, P_{RF} = -50 dBm. IF port was terminated with 300Ω impedance in the circuit simulator. For PEC boundary conversion loss was about 32 dB and for finite conductivity boundary condition, conversion loss was 35 dB.

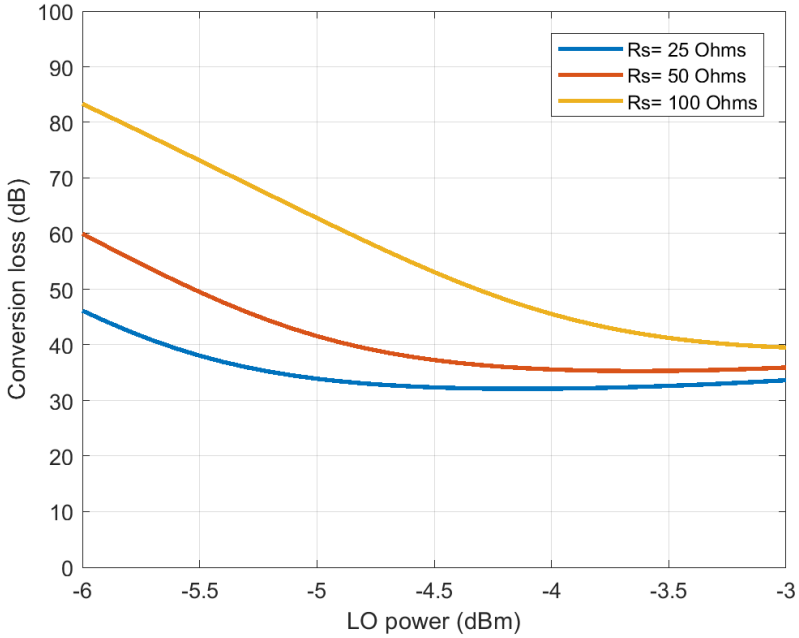

Figure 4.16: Conversion loss versus local oscillator pump power for different diode series resistance and RF power = -50 dBm

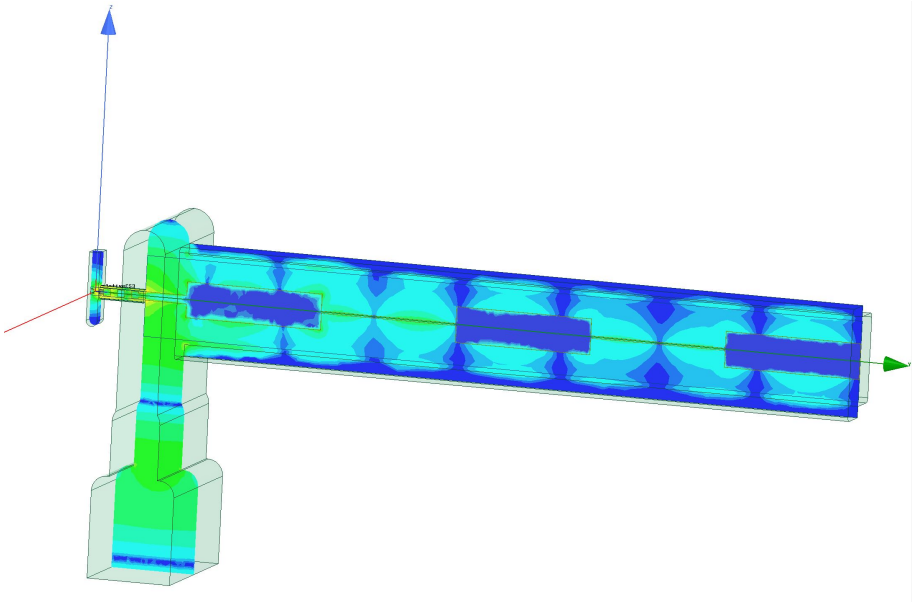

Figure 4.17: Electric field distribution in the full mixer circuitry at 585 GHz.

5

Conclusion and future work

The design and modelling of a x6 harmonic mixer operating at 3.5 THz for phase-locking of Quantum Cascade Laser (QCL) sources are presented. An ideal simulation study was carried out in the circuit simulator, four basic mixer configurations were studied and it is noticed that the Z-mixer offers minimum conversion with increased LO pump power due to the associated power dissipation in idlers. However, it is not a pure Z-mixer since the junction capacitance will provide short circuit at higher frequencies. Y-mixer offers lower conversion loss at low LO pump power and conversion nulls are observed due to destructive interference of competing mixing paths.

In-order to obtain the least conversion loss, optimum embedding impedances to be present at RF, LO and IF frequencies were calculated for ideal series resistance and also for higher arbitrary diode series resistance. Based on these, 3D-electromagnetic model was designed in a finite element method software. The simulated conversion loss was about 35 dB (including losses in the stripline and waveguide metal) for LO pump power −4 dBm, and RF power −50 dBm. This work provides initial design guidelines for x8 harmonic mixer design operating at 4.7 THz. For additional mechanical support, beam-leads will be added to the circuit structure and the 3D-electromagnetic model will be re-optimised. A tolerance analysis of the final design will be performed to understand the influence of fabrication errors on the mixer performances.

References

[1] P. H. Siegel, "Terahertz technology," *IEEE Transactions on Microwave Theory and Techniques*, vol. 50, no. 3, pp. 910–928, March 2002, DOI: 10.1109/22.989974.

[2] M. Tonouchi, "Cutting-edge terahertz technology," *Nature Photonics*, vol. 1, pp. 97–105, Feb 2007.

[3] T. G. Phillips and J. Keene, "Submillimeter astronomy (heterodyne spectroscopy)," *Proceedings of the IEEE*, vol. 80, no. 11, pp. 1662–1678, Nov 1992, DOI: 10.1109/5.175248.

[4] R. A. Pucel, "Design considerations for monolithic microwave circuits," *IEEE Transactions on Microwave Theory and Techniques*, vol. 29, no. 6, pp. 513–534, Jun 1981, DOI: 10.1109/TMTT.1981.1130387.

[5] V. Drakinskiy, P. Sobis, H. Zhao, T. Bryllert, and J. Stake, "Terahertz GaAs Schottky diode mixer and multiplier MIC's based on e-beam technology," in *2013 International Conference on Indium Phosphide and Related Materials (IPRM)*, May 2013, pp. 1–2, DOI: 10.1109/ICIPRM.2013.6562606.

[6] J. V. Siles, K. B. Cooper, C. Lee, R. H. Lin, G. Chattopadhyay, and I. Mehdi, "A new generation of room-temperature frequency-multiplied sources with up to 10× higher output power in the 160 GHz–1.6-THz range," *IEEE Transactions on Terahertz Science and Technology*, vol. 8, no. 6, pp. 596–604, Nov 2018, DOI: 10.1109/TTHZ.2018.2876620.

[7] B. S. Williams, "Terahertz quantum-cascade lasers," *Nature Photonics*, vol. 1, p. 517, Sep 2007, DOI: 10.1109/ICIPRM.2012.6403330.

[8] Heyminck, S., Graf, U. U., Güsten, R., Stutzki, J., Hübers, H. W., and Hartogh, P., "GREAT: the SOFIA high-frequency heterodyne instrument," *A&A*, vol. 542, p. L1, 2012, DOI: 10.1051/0004-6361/201218811.

[9] T. J. Pearson, R. Guesten and N. Whyborn, "Local oscillator system for the heterodyne instrument for first (HIFI)," *SPIE*, vol. 4013, July 2000.

[10] B. Swinyard, O. Auriacombe, T. Bradshaw, D. Brooks, J. Charlton, M. Crook, G. Davies, B. Ellison, M. Emes, J. Friend, D. Gerber, C. Gray, M. Henry, T. Hunt, E. Linfield, N. Navarathinam, S. Parks, T. Rawlings, S. Rea, C. Saunders, G. Savini, S. M. Tun, D. Walker, H. Wang, and B. Winter, "The low cost upper atmosphere sounder: The "elegant breadboard" programme," in *2015 8th UK, Europe, China Millimeter Waves and THz Technology Workshop (UCMMT)*, Sep. 2015, pp. 1–4, DOI: 10.1109/UCMMT.2015.7460627.

[11] J. Zmuidzinas, J. W. Kooi, J. Kawamura, G. Chattopadhyay, B. Bumble, H. G. LeDuc, and J. A. Stern, "Development of SIS mixers for 1 THz," in *Advanced*

Technology MMW, Radio, and Terahertz Telescopes, T. G. Phillips, Ed. SPIE, Jul. 1998, DOI: 10.1117/12.317386.

[12] S. Cherednichenko, S. Bevilacqua, and E. Novoselov, "THz hot-electron bolometer mixers," in *2014 39th International Conference on Infrared, Millimeter, and Terahertz waves (IRMMW-THz)*, Sep. 2014, pp. 1–3, DOI: 10.1109/IRMMW-THz.2014.6956174.

[13] K. Braun, "On the current conduction in metal sulphides (title translated from german into english," *Ann. Phys. chem.*, vol. 153, 1874, DOI: 10.1002/andp.18752291207.

[14] D. L. Sengupta, T. K. Sarkar, and D. Sen, "Centennial of the semiconductor diode detector," *Proceedings of the IEEE*, vol. 86, no. 1, pp. 235–243, Jan 1998, DOI: 10.1109/5.658775.

[15] T. W. Crowe, R. J. Mattauch, H. P. Roser, W. L. Bishop, W. C. B. Peatman, and X. Liu, "GaAs Schottky diodes for thz mixing applications," *Proceedings of the IEEE*, vol. 80, no. 11, pp. 1827–1841, Nov 1992, DOI: 10.1109/5.175258.

[16] H. Röser, H. Hübers, T. Crowe, and W. Peatman, "Nanostructure GaAs schottky diodes for far-infrared heterodyne receivers," *Infrared Physics and Technology*, vol. 35, no. 2, pp. 451 – 462, 1994, DOI: 10.1016/1350-4495(94)90102-3.

[17] P. H. Siegel, R. P. Smith, M. C. Graidis, and S. C. Martin, "2.5-THz GaAs monolithic membrane-diode mixer," *IEEE Transactions on Microwave Theory and Techniques*, vol. 47, no. 5, pp. 596–604, May 1999, DOI: 10.1109/22.763161.

[18] M. C. Gaidis, H. M. Pickett, P. H. Siegel, C. D. Smith, R. P. Smith, and S. C. Martin, "A 2.5 thz receiver front-end for spaceborne applications," in *1998 IEEE Sixth International Conference on Terahertz Electronics Proceedings. THZ 98. (Cat. No.98EX171)*, Sep. 1998, pp. 13–17, DOI: 10.1109/THZ.1998.731652.

[19] G. Chattopadhyay, "Technology, capabilities, and performance of low power terahertz sources," *IEEE Transactions on Terahertz Science and Technology*, vol. 1, no. 1, pp. 33–53, Sep. 2011, DOI: 10.1109/TTHZ.2011.2159561.

[20] H. Hubers, "Terahertz heterodyne receivers," *IEEE Journal of Selected Topics in Quantum Electronics*, vol. 14, no. 2, pp. 378–391, March 2008, DOI: 10.1109/JSTQE.2007.913964.

[21] T. Hagelschuer, N. Rothbart, H. Richter, M. Wienold, L. Schrottke, H. T. Grahn, and H.-W. Hübers, "High-spectral-resolution terahertz imaging with a quantum-cascade laser," *Opt. Express*, vol. 24, no. 13, pp. 13 839–13 849, Jun 2016, DOI: 10.1364/OE.24.013839.

[22] M. Wienold, T. Alam, L. Schrottke, H. T. Grahn, and H.-W. Hübers, "Doppler-free spectroscopy with a terahertz quantum-cascade laser," *Opt. Express*, vol. 26, no. 6, pp. 6692–6699, Mar 2018, DOI: 10.1364/OE.26.006692.

[23] M. Ravaro, C. Manquest, C. Sirtori, S. Barbieri, G. Santarelli, K. Blary, J.-F. Lampin, S. P. Khanna, and E. H. Linfield, "Phase-locking of a 2.5 thz quantum cascade laser to a frequency comb using a GaAs photomixer," *Opt. Lett.*, vol. 36, no. 20, pp. 3969–3971, Oct 2011, DOI: 10.1364/OL.36.003969.

[24] A. V. Khudchenko, D. J. Hayton, D. G. Pavelyev, A. M. Baryshev, J. R. Gao, T. Kao, Q. Hu, J. L. Reno, and V. L. Vaks, "Phase locking a 4.7 thz quantum cascade laser using a super-lattice diode as harmonic mixer," in *2014 39th Inter-*

national Conference on Infrared, Millimeter, and Terahertz waves (IRMMW-THz), Sep. 2014, pp. 1–2, DOI: 10.1109/IRMMW-THz.2014.6956455.

[25] B. T. Bulcha, J. L. Hesler, V. Drakinskiy, J. Stake, A. Valavanis, P. Dean, L. H. Li, and N. S. Barker, "Design and characterization of 1.8–3.2 THz Schottky-based harmonic mixers," *IEEE Transactions on Terahertz Science and Technology*, vol. 6, no. 5, pp. 737–746, Sep. 2016, DOI: 10.1109/TTHZ686.2016.2576,.

[26] G. Beig, "The relative importance of solar activity and anthropogenic influences on the ion composition, temperature, and associated neutrals of the middle atmosphere," *Journal of Geophysical Research: Atmospheres*, vol. 105, no. D15, pp. 19 841–19 856, Aug. 2000, DOI: 10.1029/2000jd900169.

[27] A. E. Hedin, "Extension of the MSIS thermosphere model into the middle and lower atmosphere," *Journal of Geophysical Research: Space Physics*, vol. 96, no. A2, pp. 1159–1172, Feb. 1991, DOI: 10.1029/90ja02125.

[28] W. Schottky, "Halbleitertheorie der sperrschicht," *Naturwissenschaften*, vol. 26, no. 52, pp. 843–843, Dec 1938, DOI: 10.1007/BF01774216.

[29] W. Monch, "On the physics of metal-semiconductor interfaces," *Reports on Progress in Physics*, vol. 53, no. 3, pp. 221–278, mar 1990. DOI: https://doi.org/10.1088/0034-4885/53/3/001

[30] S. Sze and K. K. Ng, *Physics of Semiconductor Devices*. John Wiley & Sons, Inc., Apr. 2006. DOI: https://doi.org/10.1002/0470068329

[31] M. Missous, E. H. Rhoderick, D. A. Woolf, and S. P. Wilkes, "On the richardson constant of intimate metal-GaAs Schottky barriers," *Semiconductor Science and Technology*, vol. 7, no. 2, pp. 218–221, feb 1992, DOI: 10.1088/0268-1242/7/2/007.

[32] J. T. Louhi and A. V. Räisänen, "On the modeling and optimization of Schottky varactor frequency multipliers at submillimeter wavelengths," *IEEE Transactions on Microwave Theory and Techniques*, vol. 43, no. 4, pp. 922–926, April 1995, DOI: 10.1109/22.375255.

[33] W. M. Kelly and G. T. Wrixon, "Conversion losses in schottky-barrier diode mixers in the submillimeter region," *IEEE Transactions on Microwave Theory and Techniques*, vol. 27, no. 7, pp. 665–672, Jul 1979.

[34] K. Bhaumik, B. Gelmont, R. J. Mattauch, and M. Shur, "Series impedance of GaAs planar Schottky diodes operated to 500 GHz," *IEEE Transactions on Microwave Theory and Techniques*, vol. 40, no. 5, pp. 880–885, May 1992, DOI: 10.1109/22.137393.

[35] M. Sotoodeh, A. H. Khalid, and A. A. Rezazadeh, "Empirical low-field mobility model for iii–v compounds applicable in device simulation codes," *Journal of Applied Physics*, vol. 87, no. 6, pp. 2890–2900, 2000, DOI: 10.1063/1.372274.

[36] K. S. Champlin and G. Eisenstein, "Cutoff frequency of submillimeter Schottky-barrier diodes," *IEEE Transactions on Microwave Theory and Techniques*, vol. 26, no. 1, pp. 31–34, Jan 1978, DOI: 10.1109/TMTT.1978.1129302.

[37] L. E. Dickens, "Spreading resistance as a function of frequency," *IEEE Transactions on Microwave Theory and Techniques*, vol. 15, no. 2, pp. 101–109, February 1967, DOI: 10.1109/TMTT.1967.1126383.

[38] A. van der Ziel, "Infrared detection and mixing in heavily doped Schottky-barrier diodes," *Journal of Applied Physics*, vol. 47, no. 5, pp. 2059–2068, May 1976. DOI: https://doi.org/10.1063/1.322936

[39] D. Pozar, *Microwave Engineering, 4th Edition.* Wiley, 2011. DOI: https://books.google.se/books?id=JegbAAAAQBAJ

[40] D. N. Held and A. R. Kerr, "Conversion loss and noise of microwave and millimeterwave mixers: Part 1 - theory," *IEEE Transactions on Microwave Theory and Techniques*, vol. 26, no. 2, pp. 49–55, Feb 1978, DOI: 10.1109/TMTT.1978.1129312.

[41] A. J. Kelly, "Fundamental limits on conversion loss of double sideband resistive mixers," *IEEE Transactions on Microwave Theory and Techniques*, vol. 25, no. 11, pp. 867–869, Nov 1977, DOI: 10.1109/TMTT.1977.1129233.

[42] M. McColl, "Conversion loss limitations on Schottky-barrier mixers (short papers)," *IEEE Transactions on Microwave Theory and Techniques*, vol. 25, no. 1, pp. 54–59, Jan 1977.

[43] J. Johnson, "Thermal agitation of electricity in conductors," *Phys. Rev.*, vol. 32, no. 1, pp. 97–109, 1928.

[44] H. Nyquist, "Thermal agitation of electric charge in conductors," *Phy. Rev.*, vol. 32, no. 1, pp. 110–113, 1928.

[45] M. J. O. Strutt, "Noise-figure reduction in mixer stages," *Proceedings of the IRE*, vol. 34, no. 12, pp. 942–950, Dec 1946, DOI: 10.1109/JRPROC.1946.232920.

[46] D. N. Held and A. R. Kerr, "Conversion loss and noise of microwave and millimeterwave mixers: Part 2 - experiment," *IEEE Transactions on Microwave Theory and Techniques*, vol. 26, no. 2, pp. 55–61, Feb 1978, DOI: 10.1109/TMTT.1978.1129313.

[47] A.A.M.Saleh, "Theory of resistive mixers," *Cambridge, MA: MIT press*, 1971.

[48] W. C. B. Peatman and T. W. Crowe, "Design and fabrication of 0.5 micron gaas schottky barrier diodes for low-noise terahertz receiver applications," *International Journal of Infrared and Millimeter Waves*, vol. 11, no. 3, pp. 355–365, Mar 1990. DOI: https://doi.org/10.1007/BF01010434

[49] W. L. Bishop, K. McKinney, R. J. Mattauch, T. W. Crowe, and G. Green, "A novel whiskerless schottky diode for millimeter and submillimeter wave application," in *1987 IEEE MTT-S International Microwave Symposium Digest*, vol. 2, May 1987, pp. 607–610.

[50] W. Y. Ali-Ahmad, W. L. Bishop, T. W. Crowe, and G. M. Rebeiz, "A 250 ghz planar low noise schottky receiver," *International Journal of Infrared and Millimeter Waves*, vol. 14, no. 4, pp. 737–748, Apr 1993. DOI: https://doi.org/10.1007/BF02084284

[51] P. Lehikoinen, J. Mallat, P. Piironen, A. Lehto, J. Tuovinene, and A. V. Räisänen, "A 119 GHz planar Schottky diode mixer for a space application," *International Journal of Infrared and Millimeter Waves*, vol. 17, no. 5, pp. 807–818, May 1996. DOI: https://doi.org/10.1007/BF02101389

[52] T. W. Crowe, "Gaas schottky barrier mixer diodes for the frequency range 1–10 thz," *International Journal of Infrared and Millimeter Waves*, vol. 10, no. 7, pp. 765–777, Jul 1989. DOI: https://doi.org/10.1007/BF01011489

[53] E. Schlecht, J. Bruston, A. Maestrini, S. Martin, D. Pukala, R. Tsang, A. Fung, R. Smith, and I. Mehdi, "200 and 400 GHz SCHOTTKY diode multipliers fabricated with integrated air-dielectric "substrateless" circuitry," 05 2000.

[54] Huan Zhao, V. Drakinskiy, P. Sobis, J. Hanning, T. Bryllert, Aik-Yean Tang, and J. Stake, "Development of a 557 GHz GaAs monolithic membrane-diode mixer," in *2012 International Conference on Indium Phosphide and Related Materials*, Aug 2012, pp. 102–105, DOI: 10.1109/ICIPRM.2012.6403330.

[55] A. Hammar, P. Sobis, V. Drakinskiy, A. Emrich, N. Wadefalk, J. Schleeh, and J. Stake, "Low noise 874 GHz receivers for the international submillimetre airborne radiometer (ISMAR)," *Review of Scientific Instruments*, vol. 89, no. 5, p. 055104, 2018, DOI: 10.1063/1.5017583.

[56] A. Y. Tang, T. Bryllert, and J. Stake, "Geometry optimization of THz sub-harmonic Schottky mixer diodes," in *2012 37th International Conference on Infrared, Millimeter, and Terahertz Waves*, Sep. 2012, pp. 1–2, DOI: 10.1109/IRMMW-THz.2012.6379506.

[57] J. F. Johansson and N. D. Whyborn, "The diagonal horn as a sub-millimeter wave antenna," *IEEE Transactions on Microwave Theory and Techniques*, vol. 40, no. 5, pp. 795–800, May 1992.

[58] P. J. Sobis, N. Wadefalk, A. Emrich, and J. Stake, "A broadband, low noise, integrated 340 GHz Schottky diode receiver," *IEEE Microwave and Wireless Components Letters*, vol. 22, no. 7, pp. 366–368, July 2012, DOI: 10.1109/LMWC.2012.2202280.

[59] M. Anderberg, P. Sobis, V. Drakinskiy, J. Schleeh, S. Dejanovic, A. Emrich, and J. Stake, "A 183-GHz Schottky diode receiver with 4 dB noise figure," in *IEEE MTT-S International Microwave Symposium (IMS)*, June 2019, pp. 172–175.

[60] N. Ridler, R. Ginley, J. Hesler, A. R. Kerr, R. D. Pollard, and D. F. Williams, "Towards standardized waveguide sizes and interfaces for submillimeter wavelengths," 03 2010.

[61] D. Jayasankar, J. Stake, and P. Sobis, "Effect of idler terminations on the conversion loss for THz Schottky diode harmonic mixers," *to be presented at the 44th International Conference on Infrared, Millimeter, and Terahertz waves (IRMMW-THz), Paris*, 2019.

[62] A. Y. Tang and J. Stake, "Impact of eddy currents and crowding effects on high-frequency losses in planar Schottky diodes," *IEEE Transactions on Electron Devices*, vol. 58, no. 10, pp. 3260–3269, Oct 2011, DOI: 10.1109/TED.2011.2160724.

[63] A. Y. Tang, E. Schlecht, R. Lin, G. Chattopadhyay, C. Lee, J. Gill, I. Mehdi, and J. Stake, "Electro-thermal model for multi-anode Schottky diode multipliers," *IEEE Transactions on Terahertz Science and Technology*, vol. 2, no. 3, pp. 290–298, May 2012, DOI: 10.1109/TTHZ.2012.2189913.

[64] L. Mania and G. Stracca, "Effects of the diode junction capacitance on the conversion loss of microwave mixers," *IEEE Transactions on Communications*, vol. 22, no. 9, pp. 1428–1435, Sep. 1974, DOI: 10.1109/10.1109/TCOM.1974.1092358.

[65] J. Hesler, D. Kurtz, and R. Feinsaugle, "The cause of conversion nulls for single-diode harmonic mixers," *IEEE Microwave and Guided Wave Letters*, vol. 9, no. 12, pp. 532–534, Dec 1999, DOI: 10.1109/75.819422.

Paper A

Effect of idler terminations on the conversion loss for THz Schottky diode harmonic mixers

D. Jayasankar, J. Stake, and P. Sobis
to be presented at the *44th International Conference on Infrared, Millimeter, and Terahertz waves(IRMMW-THz), Paris, Sep 2019.*

Effect of idler terminations on the conversion loss for THz Schottky diode harmonic mixers

Divya Jayasankar[1], Jan Stake[1], and Peter Sobis[2]

[1]Terahertz and Millimetre Wave Laboratory, Department of Microtechnology and Nanoscience, Chalmers University of Technology, SE-41296 Göteborg, Sweden
[2]Omnisys Instruments AB, SE-42132 Västra Frölunda, Sweden

***Abstract*—Efficient and reliable frequency converters, preferably operating at room temperature, are critical components for frequency-stabilizing terahertz sources. In this work, we present the analysis of optimum configurations for Schottky diode based x4, x6, and x8 harmonic mixers operating at 2.3 THz, 3.5 THz, and 4.7 THz respectively. Detailed large-signal analysis of the two basic single-ended Z- and Y-mixers was carried out using a standard Schottky-diode model. For each case, the conversion loss was minimized by finding optimal embedding impedances at RF, LO, and IF frequencies. The analysis shows that the Y-mixer has less conversion loss at a low LO pump power. However, the Z-mixer provides reduced loss with increasing harmonic index and pump power due to the associated power dissipation in idler circuits. The results provide preliminary design guidelines for room- temperature frequency converters and their use in phase-locked loop applications.**

Index terms - Harmonic mixers, Phase locking, QCL, Schottky diodes

I. Introduction

SCHOTTKY diode based frequency converters offer wide instantaneous bandwidth, low spurious response and high conversion efficiency, thereby a suitable component for phase-locked loop applications. For instance, frequency stabilization of local oscillator sources, e.g. Quantum Cascade Lasers (QCLs), is crucial for high-resolution heterodyne instrumentation at terahertz frequencies. Phase-locking of terahertz sources using microwave component provides highly stable and precise reference frequency and a compact solution, which are important for spaceborne instrumentation. This approach was demonstrated by Betz. et. al [1] and Bulcha et. al using Schottky diode based harmonic mixers [2] and by Hayton et. al using super-lattice diode mixer [3].

Much research has estimated the theoretical limit on conversion loss for fundamental diode mixers [4]. However, less attention has been paid to the harmonic mixers, as conversion loss degrades with increasing harmonic index. The purpose of this ideal simulation study is to analyse the minimum conversion loss that can be obtained for x4, x6, and x8 harmonic mixers with reactive out-of-band frequency terminations [5].

This paper is structured as follows. Section II focuses on the simulation setup in the circuit simulator and comparison of the analytical model with the diode I-V measurement. Section III presents the ideal conversion loss for x4, x6, and x8 harmonic mixers and also the optimum embedding impedance at LO and RF frequencies for two basic mixer topology (Z-, and Y-mixers).

II. Methodology

For the single anode Schottky diode shown in figure 1, we apply an equivalent quasi-static Schottky-diode model, which consists of a non-linear junction capacitance (C_j), a parallel non-linear current source (I-V) and a series resistance (R_s). Extrinsic parasitics and high-frequency effects are excluded [6] and considered to be part of the embedding circuit and the effect of self-heating is not included [7]. For small anode diameters, it is important to add the first-order fringing effect to the junction capacitance model [8]. Series resistance was estimated from the measurement results and FEM simulation. Based on these analytical models, a dc-simulation was setup and figure 1 shows the I-V plot of the in-built diode model with $R_s = 23\,\Omega$, $\eta = 1.2$, $C_{j0} = 0.47\,\text{fF}$ and $I_{sat} = 1\,\text{fA}$, $N_{d,epi} = 5 \times 10^{17}\,\text{cm}^{-3}$ for $0.15\,\mu\text{m}^2$ anode area.

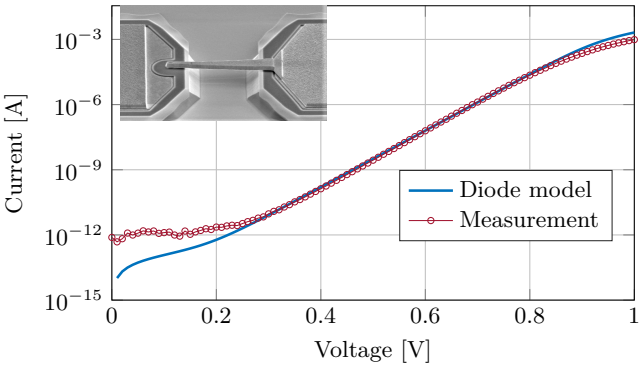

Fig. 1: Measurement and model of the I-V characteristics of an in-house Schottky diode with $0.15\,\mu\text{m}^2$ anode area. The measurement was performed with Kelvin probes at room-temperature (dark condition).

Harmonic balance simulation was performed to study basic single-ended Z- and Y-mixer topologies [5]. Different harmonic mixers (x4, x6, and x8) were studied for a LO frequency of 585 GHz and IF of 10 GHz. The DC-voltage across the diode was kept at zero and all the out-of-band frequencies (idlers) were terminated either as short (Y-mixer) or open (Z-mixer), RF power was set to $-50\,\text{dBm}$. Note at high frequencies, the junction capacitance will be a short therefore it is not a pure Z-mixer [9].

III. Results

Two basic mixer topologies were studied and results are presented in figure 2 for $0.15\,\mu\text{m}^2$ anode area. It can be seen that, for low LO pump power, Y-mixer (short) yields low conversion loss. On the other hand, the Z-mixer (open) gives reduced loss as the pump power increases since there is no power dissipated in the idler circuits. Due to destructive interference between mixing products, conversion nulls are observed in single-ended harmonic diode mixers [10] for Y-mixers as shown in figure 2.

Figure 3 and 4 shows the optimum embedding impedances at LO and RF frequencies respectively that offers minimum conversion loss for Y-, Z-mixer configuration for x4, x6,and x8 harmonic mixers. For low LO power (−20 dBm), the optimum embedding impedances are equal to the small-signal impedance of the diode equivalent circuit. For the x6 harmonic mixer, typical optimum IF impedance is 1200 Ω and 600 Ω for Z- and Y-mixer respectively. Optimum embedding LO and RF impedances for different LO operating power provide useful insights while designing the mixer circuitry.

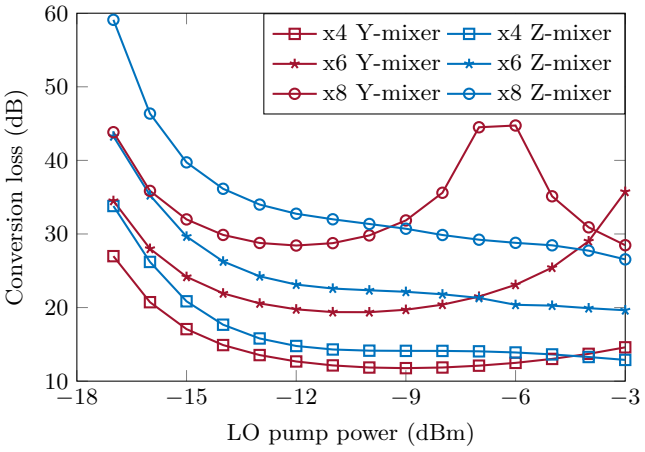

Fig. 2: Conversion loss vs. LO power for 0.15 µm^2 anode contact area for Z- and Y-mixer operating at 585 GHz LO frequency and 2.3 THz, 3.5 THz, and 4.7 THz RF frequency.

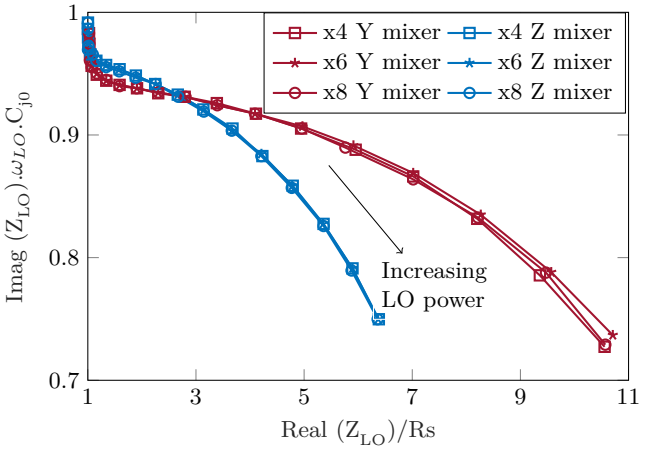

Fig. 3: Optimum LO embedding impedance at 585 GHz plotted for x4, x6, and x8 harmonic mixers in Z-, and Y-mixer configuration in Z-plane for LO power sweep from −20 dBm to −3 dBm. $R_s = 23\,\Omega$ is the diode series resistance and $C_{j0} = 0.47$ fF is the zero-bias junction capacitance.

IV. Acknowledgment

Authors would like to thank Dr. Tomas Bryllert, Dr. Josip Vukusic, Dr. Elena Saenz and Dr. Heinz-Wilhelm Hübers for fruitful discussions. This research was carried out in the Gigahertz Centre in a project financed by ESA under the contract No. 4000125911/18/NL/AF "Frequency stabilisation of a Quantum Cascade Laser for Supra-THz applications" and Swedish National Space Board under the contract No. 170/17 "THz Schottky diode mixers for high-resolution FIR spectroscopy".

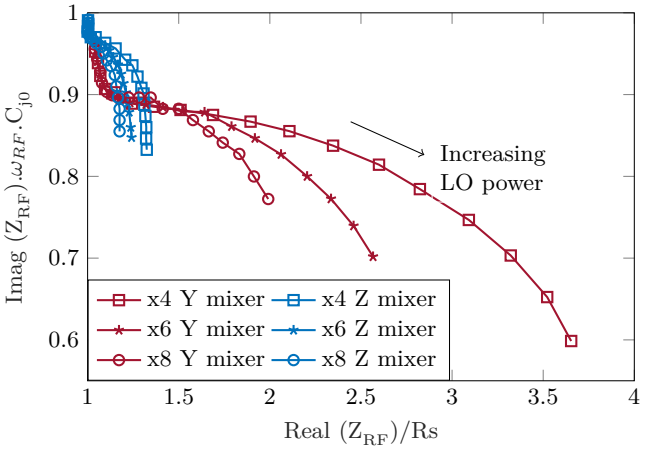

Fig. 4: Optimum embedding RF impedance plotted for x4, x6, and x8 harmonic mixers in Z-, and Y-mixer configuration in Z-plane for LO power sweep from −20 dBm to −3 dBm, $R_s = 23\,\Omega$ and $C_{j0} = 0.47$ fF $\omega_{RF} = n.\omega_{LO} - \omega_{IF}$, where n is the harmonic index.

References

[1] A. L. Betz, R. T. Boreiko, B. S. Williams, S. Kumar, Q. Hu, and J. L. Reno, "Frequency and phase-lock control of a 3 THz quantum cascade laser," *Opt. Lett.*, vol. 30, no. 14, pp. 1837–1839, Jul 2005.

[2] B. T. Bulcha, J. L. Hesler, V. Drakinskiy, J. Stake, A. Valavanis, P. Dean, L. H. Li, and N. S. Barker, "Design and characterization of 1.8–3.2 THz schottky-based harmonic mixers," *IEEE Transactions on Terahertz Science and Technology*, vol. 6, no. 5, pp. 737–746, Sep. 2016, DOI: 10.1109/TTHZ686.2016.2576.

[3] D. Hayton, A. Khudchencko, D. Pavelyev, J. Hovenier, A. Baryshev, J. Gao, T. Kao, Q. Hu, J. Reno, and V. Vaks, "Phase locking of a 3.4 THz third-order distributed feedback quantum cascade laser using a room-temperature superlattice harmonic mixer," *Applied Physics Letters*, vol. 103, no. 5, 7 2013, DOI: 10.1063/1.4817319.

[4] A. J. Kelly, "Fundamental limits on conversion loss of double sideband resistive mixers," *IEEE Transactions on Microwave Theory and Techniques*, vol. 25, no. 11, pp. 867–869, Nov 1977, DOI: 10.1109/TMTT.1977.1129233,.

[5] A.A.M.Saleh, "Theory of resistive mixers," *MIT press*, 1971.

[6] A. Y. Tang and J. Stake, "Impact of eddy currents and crowding effects on high-frequency losses in planar schottky diodes," *IEEE Transactions on Electron Devices*, vol. 58, no. 10, pp. 3260–3269, Oct 2011, DOI: 10.1109/TED.2011.2160724.

[7] A. Y. Tang, E. Schlecht, R. Lin, G. Chattopadhyay, C. Lee, J. Gill, I. Mehdi, and J. Stake, "Electro-thermal model for multi-anode schottky diode multipliers," *IEEE Transactions on Terahertz Science and Technology*, vol. 2, no. 3, pp. 290–298, May 2012, DOI: 10.1109/TTHZ.2012.2189913,.

[8] J. T. Louhi and A. V. Räisänen, "On the modeling and optimization of Schottky varactor frequency multipliers at submillimeter wavelengths," *IEEE Transactions on Microwave Theory and Techniques*, vol. 43, no. 4, pp. 922–926, 1995.

[9] L. Mania and G. Stracca, "Effects of the diode junction capacitance on the conversion loss of microwave mixers," *IEEE Transactions on Communications*, vol. 22, no. 9, pp. 1428–1435, 1974.

[10] J. Hesler, D. Kurtz, and R. Feinsaugle, "The cause of conversion nulls for single-diode harmonic mixers," *IEEE Microwave and Guided Wave Letters*, vol. 9, no. 12, pp. 532–534, Dec 1999, DOI: 10.1109/75.819422.

Paper B

Development of supra-terahertz Schottky diode mixers

D. Jayasankar, V. Drakinskiy, P. Sobis, J. Stake
to be presented at the *IEEE International Microwave and RF Conference (IMaRC), Mumbai, Dec 2019.*

Development of supra-terahertz Schottky diode mixers

Divya Jayasankar[1], Vladimir Drakinskiy[1], Peter Sobis[2], and Jan Stake[1]

[1]Terahertz and Millimetre Wave Laboratory, Department of Microtechnology and Nanoscience, Chalmers University of Technology, SE-41296 Göteborg, Sweden
[2]Omnisys Instruments AB, SE-42132 Västra Frölunda, Sweden

***Abstract*—Room temperature and broadband Schottky diode mixers for terahertz sensing and phase-locking of far-infrared optical sources (e.g. quantum cascade laser) are crucial for heterodyne instrumentation for air/space-borne applications. In this paper, we present the development of fundamental single-ended Schottky diode mixers in the frequency range 3 - 5 THz. The design is based on Schottky diodes with sub-micron anode area, defined using nano lithography techniques, and integrated with suspended striplines on an ultra-thin GaAs-membrane.**

Index terms - Frequency converters, heterodyne receivers, horn antennas, mixers, phase locking, Schottky diodes, sub-millimeter wave electronics.

I. Introduction

SCHOTTKY diode technology is the workhorse for low noise and broadband sub-millimetre wave heterodyne radiometers, operating at ambient temperatures [1]. In particular, the future scientific objectives and instrument requirements for Earth observation are driven by the need to accommodate the atmospheric measurement of atomic oxygen (OI) and hydroxyl radical (OH) lines at 3.5 THz and 4.7 THz, respectively, and perform data collection over a long period. Hence, there is a strong need for compact terahertz heterodyne receivers with high spectral resolution and able to operate without any cryogenic cooling. Compared to ultra-low noise terahertz technology (SIS- or HEB mixers), the GaAs Schottky diode technology can operate over a wide temperature range and instantaneous bandwidth (IF) and hence well suited for long lifetime missions. However, the lack of efficient and compact power sources [2] above 2 THz, is one of the limiting factors that restrict the realization of un-cooled heterodyne receivers at higher frequencies [3].

Integrated and planar Schottky diode technology was developed during the 90s [4] opened up for more reliable and advanced terahertz mixers and multipliers compared to previous whisker-contacted devices [5]. In 1999, Siegel et al.[6] demonstrated membrane based technology that allows for low electrical parasitics and operation at terahertz frequencies. Based on this monolithic membrane diode technology, the first planar 2.5 THz Schottky diode heterodyne receiver was developed for a NASA spaceflight mission using a CO_2-pumped methanol far-infrared laser [7]. Over the past decade, Quantum Cascade Lasers (QCLs) has shown steady improvement in performance [8], thereby making it an ideal candidate as a compact local oscillator source at ambient temperatures, which is feasible with passive cooling for space borne instrumentation. hence, fundamental Schottky diode receivers beyond 3 THz are foreseen thanks to the development of far-infrared quantum cascade lasers. However, QCLs are prone to frequency instabilities and hence requires a frequency stabilization scheme [9]. For this, a harmonic mixer is a vital part of the frequency stabilization loop, and should preferably be stable and easy to integrate. Hence, Schottky-diode based harmonic mixer that offers wide instantaneous bandwidth, low spurious response and high conversion efficiency is a strong candidate for frequency stabilization of terahertz oscillators. Bulcha et al. have demonstrated Schottky-diode based harmonic mixer for phase locking of a 2.5 THz QCL [10] and Hayton et al. has demonstrated phase-locking at 3.4 THz using a super-lattice diode mixer [11]. In overall, there is a need to develop fundamental mixers and harmonic mixers that are qualified for space-borne heterodyne receivers up to 4.7 THz.

In this paper, we will present the development of fundamental mixers at 3.5 THz, using Chalmers in-house integrated diode technology [12], and in-house precision machining of waveguide housing. The paper is structured as follows: Section IIA describes diode technology and modelling. Section IIB gives a brief introduction about simulation set up in circuit simulator to find the optimum embedding impedances at RF, LO and IF frequencies. Section IIC gives an overview of mixer circuitry design. Finally, section III describes preliminary simulation results and discussion on how the design can be scaled to 4.7 THz.

II. Methodology

The 3.5 THz mixer is designed to be pumped with a quantum cascade laser providing circa 2 mW of signal power. The transmission loss in waveguides, including horn antennas, are very high at terahertz frequencies and it is therefore essential to find a compact circuit solution with short access waveguides. Moreover, the short wavelengths (86 µm) set narrow fabrication tolerances. Therefore, a single ended mixer topology was chosen using combined LO/RF port, and a standard RF/LO choke filter for the IF port (and dc-bias). A horn antenna will be integrated and part of the waveguide housing as well as a low noise amplifier MMIC for the IF signal [13].

A. Diode technology and modeling

Realization of circuits at high frequencies are often limited due to the existence of higher order propagating modes in the supporting GaAs substrate. In-order to reduce the circuit losses and parasitics, the integrated diode technology will be realized using suspended stripline technology in 2 µm thick GaAs membrane [12]. The Chalmers Schottky diode process has shown state-of-the-art performance in various receivers between 183 GHz and 3 THz [10], [14], [15].

For a single anode diode as shown in figure 1, an equivalent quasi-static equivalent Schottky-diode model of the intrinsic part is applied. It consists of diode series resistance (R_s), junction capacitance (C_j) and non-linear current source (g_m). Analytical series resistance model takes into account of contributions from un-depleted epi-layer with doping concentration $5 \times 10^{17}\,\mathrm{cm}^{-3}$, highly-doped buffer layer and ohmic contact.

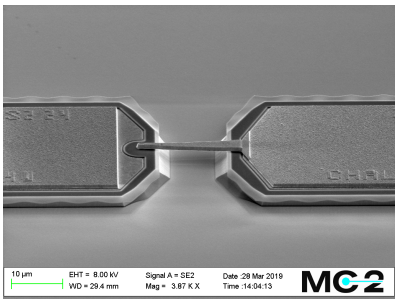

Fig. 1: Scanned Electron Microscope picture of single-anode Schottky diode fabricated at Chalmers University of Technology

Extrinsic parasitics are considered to be part of the embedding circuit, high-frequency effects are excluded [16] and effects of self-heating is not included [17]. The non-linear junction capacitance includes the effect of first-order fringing effect as shown below [18]

$$C_{j0} = \frac{\epsilon_s A}{W_d}\left(1 + b\left(\frac{W_d}{R_{anode}}\right)\right) \tag{1}$$

where, A is the anode contact area, R_{anode} is radius of the anode contact, b is numerical constant 1.5 and (W_d) is the depletion width at zero bias.

B. Optimum embedding impedances

In-order to find the optimum embedding impedances at RF/LO and IF frequencies that offers least conversion loss, ideal large-signal simulation study was carried out [19]. The above analytical diode model with $R_S = 25\,\Omega$, $C_{j0} = 0.47\,\text{fF}$, $\eta = 1.2$, $I_{sat} = 1\,\text{fA}$ and anode area $0.15\,\mu\text{m}^2$ together with short circuit out of band termination (Y-mixer) were employed. Figure 2, shows the optimum embedding impedances at RF, LO and IF frequencies for various local oscillator driving power and without any dc-bias.

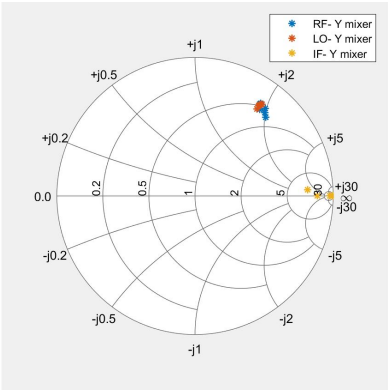

Fig. 2: Smith chart showing optimum embedding impedances at RF, LO and IF frequencies in Y-mixer configuration where idlers are short circuited

C. Design of Supra-THz Mixers

The 3.5 THz mixer circuitry is designed in a E-plane split waveguide block, figure 3 shows the full 3D-electromagnetic model of Schottky diode placed inside a E-plane split RF/LO waveguide block, waveguide-channel and RF/LO choke filters implemented as high-low impedance striplines. Dimensions of the input waveguide (50 µm x 25 µm) were chosen such that the aspect ratio is 1x1 which eases the waveguide milling process and cut-off frequency is 3 THz.

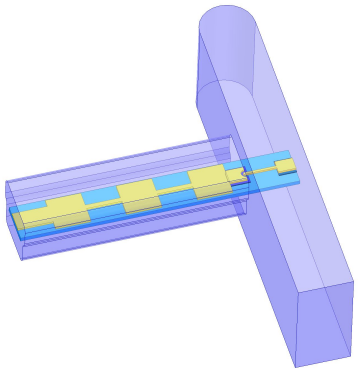

Fig. 3: 3D EM model of the RF waveguide with Schottky-diode and RF 'Band-stop' filter.

To present the optimum embedding impedance at RF/LO frequency, and to maximize the energy that couples from input port to the diode, geometry optimization of the Schottky diode and tuning of back-short distance was carried out. Waveguide-channel dimensions were varied using parametric sweep and optimized, so that only fundamental quasi-TEM mode propagates along the stripline filter. The high-low impedance stripline sections, acts as a band-stop filter that presents a short-circuit to the RF/LO signal and has a simulated rejection of about −18 dB. The S-parameter from 3D-electromagnetic model is exported to a non-linear harmonic balance circuit simulation, to evaluate the conversion loss of the circuit as shown in figure 4. Losses from the waveguide walls are excluded in this simulation, only losses from the striplines were taken into account.

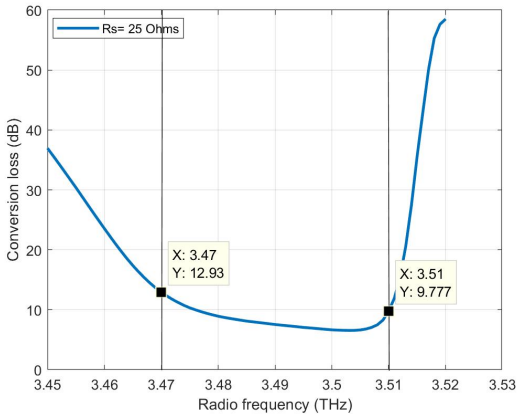

Fig. 4: Conversion loss versus radio frequency for different LO pump power

III. Results

Figure 4 shows the ideal conversion loss versus radio frequency without access waveguide losses. For the final submission and conference presentation, we will present the final design at 3.5 THz, including integrated horn antenna, as well

as predicted mixer performance including a more realistic loss estimate. In addition, progress on 4.7 THz designs and harmonic mixers will be presented.

IV. Acknowledgment

Authors would like to thank Dr. Tomas Bryllert, Dr. Josip Vukusic, Dr. Elena Saenz and Dr. Heinz-Wilhelm Hübers for fruitful discussions. This research was carried out in the Gigahertz Centre in a project financed by ESA under the contract No. 4000125911/18/NL/AF "Frequency stabilisation of a Quantum Cascade Laser for Supra-THz applications" and Swedish National Space Board under the contract No. 170/17 "THz Schottky diode mixers for high-resolution FIR spectroscopy".

References

[1] I. Mehdi, J. V. Siles, C. Lee, and E. Schlecht, "THz Diode Technology: Status, Prospects, and Applications," *Proceedings of the IEEE*, vol. 105, no. 6, pp. 990–1007, June 2017, DOI: 10.1109/JPROC.2017.2650235.

[2] G. Chattopadhyay, "Technology, capabilities, and performance of low power terahertz sources," *IEEE Transactions on Terahertz Science and Technology*, vol. 1, no. 1, pp. 33–53, Sep. 2011, DOI: 10.1109/TTHZ.2011.2159561.

[3] H. Hubers, "Terahertz heterodyne receivers," *IEEE Journal of Selected Topics in Quantum Electronics*, vol. 14, no. 2, pp. 378–391, March 2008, DOI: 10.1109/JSTQE.2007.913964.

[4] T. W. Crowe, R. J. Mattauch, H. P. Roser, W. L. Bishop, W. C. B. Peatman, and X. Liu, "Gaas schottky diodes for thz mixing applications," *Proceedings of the IEEE*, vol. 80, no. 11, pp. 1827–1841, Nov 1992, DOI: 10.1109/5.175258.

[5] H. Röser, H. Hübers, T. Crowe, and W. Peatman, "Nanostructure gaas schottky diodes for far-infrared heterodyne receivers," *Infrared Physics and Technology*, vol. 35, no. 2, pp. 451 – 462, 1994, DOI: 10.1016/1350-4495(94)90102-3.

[6] P. H. Siegel, R. P. Smith, M. C. Graidis, and S. C. Martin, "2.5-THz GaAs monolithic membrane-diode mixer," *IEEE Transactions on Microwave Theory and Techniques*, vol. 47, no. 5, pp. 596–604, 1999, DOI: 10.1109/22.763161.

[7] M. C. Gaidis, H. M. Pickett, P. H. Siegel, C. D. Smith, R. P. Smith, and S. C. Martin, "A 2.5 thz receiver front-end for spaceborne applications," in *1998 IEEE Sixth International Conference on Terahertz Electronics Proceedings. THZ 98. (Cat. No.98EX171)*, Sep. 1998, pp. 13–17, DOI: 10.1109/THZ.1998.731652.

[8] B. S. Williams, "Terahertz quantum-cascade lasers," *Nature Photonics*, vol. 1, p. 517, Sep 2007, DOI: 10.1109/ICIPRM.2012.6403330.

[9] A. L. Betz, R. T. Boreiko, B. S. Williams, S. Kumar, Q. Hu, and J. L. Reno, "Frequency and phase-lock control of a 3 THz quantum cascade laser," *Opt. Lett.*, vol. 30, no. 14, pp. 1837–1839, Jul 2005, DOI: 10.1364/OL.30.001837,.

[10] B. T. Bulcha, J. L. Hesler, V. Drakinskiy, J. Stake, A. Valavanis, P. Dean, L. H. Li, and N. S. Barker, "Design and characterization of 1.8–3.2 THz schottky-based harmonic mixers," *IEEE Transactions on Terahertz Science and Technology*, vol. 6, no. 5, pp. 737–746, Sep. 2016, DOI: 10.1109/TTHZ686.2016.2576.

[11] D. Hayton, A. Khudchencko, D. Pavelyev, J. Hovenier, A. Baryshev, J. Gao, T. Kao, Q. Hu, J. Reno, and V. Vaks, "Phase locking of a 3.4 THz third-order distributed feedback quantum cascade laser using a room-temperature superlattice harmonic mixer," *Applied Physics Letters*, vol. 103, no. 5, 7 2013, DOI: 10.1063/1.4817319,.

[12] V. Drakinskiy, P. Sobis, H. Zhao, T. Bryllert, and J. Stake, "Terahertz GaAs Schottky diode mixer and multiplier MIC's based on e-beam technology," in *2013 International Conference on Indium Phosphide and Related Materials (IPRM)*, May 2013, pp. 1–2, DOI: 10.1109/ICIPRM.2013.6562606.

[13] P. J. Sobis, N. Wadefalk, A. Emrich, and J. Stake, "A broadband, low noise, integrated 340 GHz Schottky diode receiver," *IEEE Microwave and Wireless Components Letters*, vol. 22, no. 7, pp. 366–368, July 2012, DOI: 10.1109/LMWC.2012.2202280.

[14] M. Anderberg, P. Sobis, V. Drakinskiy, J. Schleeh, S. Dejanovic, A. Emrich, and J. Stake, "A 183-GHz Schottky diode receiver with 4 dB noise figure," in *IEEE MTT-S International Microwave Symposium (IMS)*, June 2019, pp. 172–175.

[15] A. Hammar, P. Sobis, V. Drakinskiy, A. Emrich, N. Wadefalk, J. Schleeh, and J. Stake, "Low noise 874 ghz receivers for the international submillimetre airborne radiometer (ISMAR)," *Review of Scientific Instruments*, vol. 89, no. 5, p. 055104, 2018, DOI: 10.1063/1.5017583.

[16] A. Y. Tang and J. Stake, "Impact of eddy currents and crowding effects on high-frequency losses in planar schottky diodes," *IEEE Transactions on Electron Devices*, vol. 58, no. 10, pp. 3260–3269, Oct 2011, DOI: 10.1109/TED.2011.2160724.

[17] A. Y. Tang, E. Schlecht, R. Lin, G. Chattopadhyay, C. Lee, J. Gill, I. Mehdi, and J. Stake, "Electro-thermal model for multi-anode schottky diode multipliers," *IEEE Transactions on Terahertz Science and Technology*, vol. 2, no. 3, pp. 290–298, May 2012, DOI: 10.1109/TTHZ.2012.2189913.

[18] J. T. Louhi and A. V. Räisänen, "On the modeling and optimization of Schottky varactor frequency multipliers at submillimeter wavelengths," *IEEE Transactions on Microwave Theory and Techniques*, vol. 43, no. 4, pp. 922–926, April 1995, DOI: 10.1109/22.375255.

[19] D. Jayasankar, J. Stake, and P. Sobis, "Effect of idler terminations on the conversion loss for thz schottky diode harmonic mixers," in *to be presented at the 44th International Conference on Infrared, Millimeter, and Terahertz waves (IRMMW-THz), Paris*, 2019.